NOVEL HEAT TREATMENT APPLICATIONS FOR CONCENTRICALLY BRACED FRAMES

NOVEL HEAT TREATMENT APPLICATIONS FOR CONCENTRICALLY BRACED FRAMES

By

HOSSEIN MOHAMMADI, M.Sc., B.Sc.

A Thesis Submitted to the School of Graduate Studies in Partial Fulfilment of the Requirements for the Degree Master of Applied Science

McMaster University

MASTER OF APPLIED SCIENCE (2018) (Civil Engineering)

McMaster University Hamilton, Ontario

TITLE: Novel Heat Treatment Applications in Designing Gusset Plate Connections and Braces

AUTHOR: HOSSEIN MOHAMMADI, M.Sc. (Sharif University of Technology, Tehran, Iran)

SUPERVISOR: Dr. Tracy C. Becker

NUMBER OF PAGES: x, 62

ABSTRACT

Concentrically braced frames (CBFs) have been widely used in seismic areas as efficient structural systems to provide both lateral stiffness and strength. They dissipate earthquake energy through the inelastic deformation of the braces in both tension and compression. While these frames are efficient in providing lateral stiffness and strength, their inelastic mechanism is not ductile when compared to other systems such as moment resisting frames (MRFs). This student proposes a new approach to enhance the ductile behavior of CBFs by locally heat treating gusset plate connections or braces. In this method, the steel is heated locally to austenitizing temperature and then cooled with the appropriate rate to achieve the desired material properties.

In gusset plate connections, to permit the rotation imposed from brace buckling, the conventional approach is to use linear fold lines, which can result in overly large plates. A more compact design uses elliptical fold lines, but both designs can lead to damage to welds with surrounding components. To enhance the performance of the gusset plate connection, a yield path is defined with a locally weakened zone within a high strength steel gusset plate. The weakened zone, created through heat treatment concentrated the inelastic deformation, resulting in an efficiently sized connection in which the failure mechanism is tightly controlled. A design methodology for the heat treated gusset plate is proposed, and finite element analysis is used to analyze the behavior of the heat treated gusset plates.

In conventional braces, repeated buckling leads to deterioration and low-cycle fatigue which limits the ductility capacity of the CBF, compared to MRFs. As a novel approach,

heat treatment is used to increase the local yield strength in the brace. Through this method, the buckling is permitted to occur, but an enhancement in the buckling behavior is intended. Various heat treated configurations are investigated, and finite element analysis is used to compare the behavior of heat treated braces.

ACKNOWLEDGEMENTS

First and foremost, I wish to thank my supervisor Dr. Tracy Becker for her support and guidance throughout this research. Studying and working under her supervision was an asset for me to deepen my understanding in earthquake and structural engineering. I would also like to thank Dr. Hatem Zurob for sharing his expertise in material science with me in a simple language. Having his help, I learnt quite a bit about steel materials.

Thanks to the great technicians Doug Culley, Xiaogang Li, Mike Bruhis, and Kent Wheeler, and research associates Florent Lefevre-Schlick and Hamid Azizi for all their advice and assistance during my research. Without them, this project would not have been done.

I would like to thank Sarah Sullivan, Joanne Gadawski, and Tonya Antonecchia, the amazing staff of the Civil Engineering Department. I always saw them helping the students including me enthusiastically and passionately.

Thank you to my significant other, Vicky, and my dearest friends Mehdi Shafikhani, Mohammadreza Najafi, Amin Halali, Reza Pazouki, and Nojan Shafikhani. With you, I have had great moments.

Finally, I need to thank my parents, to whom I owe everything.

TABLE OF CONTENT

LIST OF FIGURES

LIST OF TABLES

CHAPTER1: INTRODUCTION

After the Northridge earthquake, there was an increase in the use of concentrically braced frames (CBFs). Providing strength and lateral stiffness, CBFs are economical systems to control drifts [1], which has made them a commonly used lateral load resisting system. A typical CBF with a diagonal brace and rectangular gusset plate is shown in Figure 1.1. In small, frequent service-level seismic events, these systems remain nearly elastic. However, in large infrequent earthquakes, these systems dissipate energy through axial tensile yielding and buckling deformation of the braces. A major shortcoming of this system is the brace fracture after repeated buckling and the low ductility, when compared to MRFs.

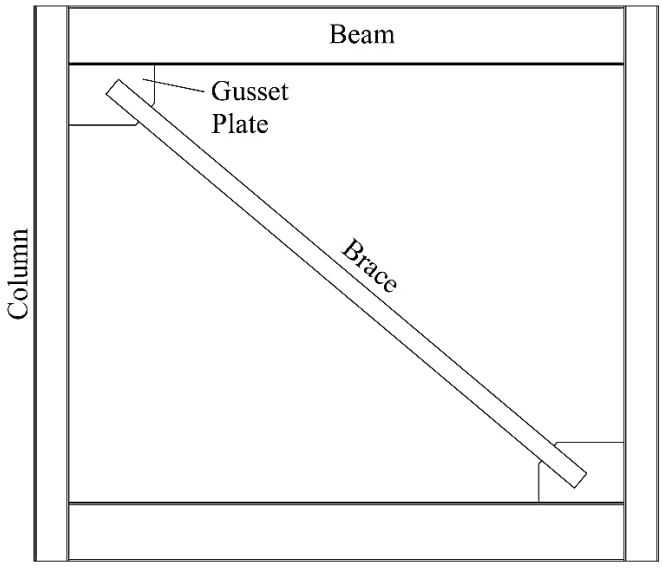

Figure 1.1: A typical CBF with diagonal brace and rectangular gusset plates

The steel types commonly used as structural sections and plates in civil construction in North America are shown in Table 1.1 [2, 3]. These normal steel types can reach an elongation of almost 20%. In recent years, high strength steel structural sections with tensile

strength ranging from 750 MPa to 1250 Mpa have been increasingly used for structural engineering purposes such as circular steel tubes and concrete-filled tubes especially in high rise buildings [4, 5]. However, structural high strength steel has significantly less ductility capacity and fatigue resistance [6]. With an increase of yield strength of steel braces, the compressive bearing capacity would be governed by buckling behavior. Hence, the tensile and compressive capacities would become more disproportionate than for normal steel, resulting in the development of severe unbalanced forces in surrounding elements. Stability would also be a problem for thinner high strength gusset plates. However, by changing the local material properties, benefits from both high and normal strength steel may be gained.

Table 1.1: Steel types and mechanical properties of structural sections and plates

Reference	Structural section	Steel type	Yield strength (F_y)	Tensile strength (F_u)
AISC **[2]**	Wide flange section (W)	A992	345	450
	Hollow structural section (HSS)	A500 Grade C	317-345	427
	Plates	A572 Grade 50	345	450
		A36	250	400
CISC **[3]**	Wide flange section (W)	A992	345	450
	Hollow structural section (HSS)	G40.21 350W	350	450
	Plates	G40.21 300W	300	450

1.1. Heat Treatment

Heat treatment is not a new technology; however, it is a relatively novel method in structural engineering, especially for seismic design. Morrison et al. [7] used heat treatment to reduce the strength and increase the ductility of A992 steel to develop a “heated beam

section" (HBS) for moment frames. Similar to reduced beam sections, the beam flanges slightly away from the column face are weakened using electric surface heating pads. Yu et al. [8] investigated HBS with Q345B steel (Chinese code) for concrete filled rectangular tube connections to address problems with stress concentration in the beam flanges due to column welding. Morrison et al. [9] also used the HBS concept to address ductility deficiencies in welded unreinforced flange-bolted web (WUF-B) connection. The modified connection showed a shifting of yielding and buckling away from the critical zone of the connection. Yu et al. [10] used heat treatment to propose weakened portions of steel plate shear walls. While steel coupons were heated and tested, the heat treatment for the shear wall was done through finite element simulation. They found that striped strength-reduction zones could improve plasticity distribution and minimize boundary zone stress concentrations without significant loss of the strength and lateral stiffness.

The steel microstructure determines the mechanical properties of the steel material, including both strength and ductility. The microstructure can be transformed through heating and cooling patterns (Figure 1.2), with one of the most important parameters being the cooling rate. Figure 1.2b shows a continuous cooling transformation (CCT) diagram for steel A514 generated with the CCT Diagram Module of MCASIS v2.1 [11]. It is shown that from the austenitizing temperature, quick quenching results in creation of martensite, which has the highest strength and most brittle microstructure, while a controlled slow cooling leads to a coarser and larger grain structure, resulting in pearlite, which is softer and more ductile. Therefore, a sufficiently slow cooling rate is desirable to lower the steel strength while maintaining or increasing the ductility.

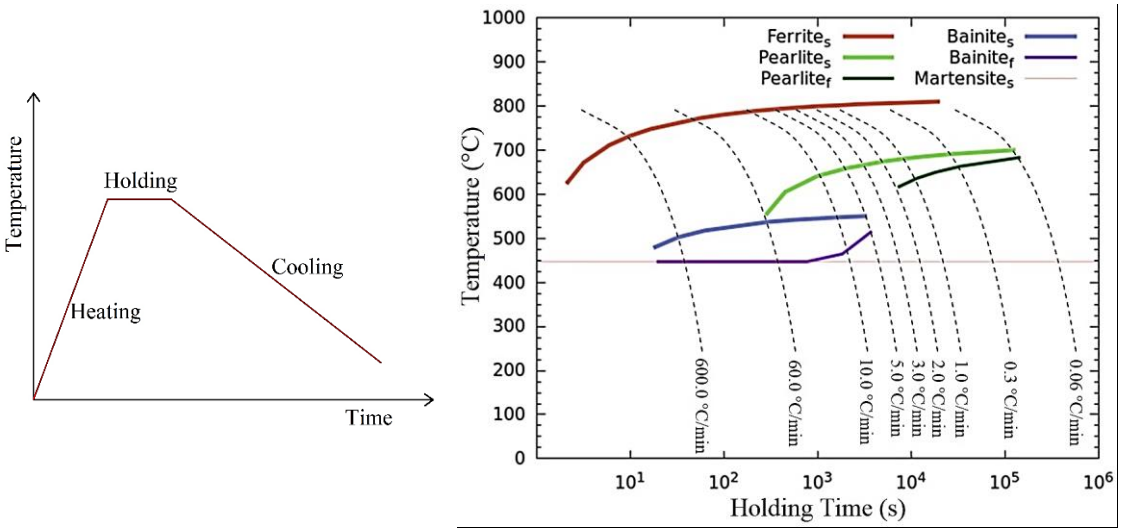

(a) (b)

Figure 1.2: Annealing heat treatment. (a) General heat treatment procedure (b) Continuous-cooling-transformation for steel A514 with 0.12% carbon.

1.2. Gusset Plate

To facilitate brace buckling, the gusset plates must undergo large inelastic rotations with simultaneous tensile or compressive loading without premature failure [12]. This is most often achieved through designing the gusset plate with a $2t_p$ free width between the restrained gusset line and the brace end, where t_p is the gusset plate thickness (Figure 1.3a). This ensures the free out-of-plane rotation of the gusset plate during brace buckling and prevents damage accumulation in the surrounding connection [13-15]. This linear clearance works well; however, it leads to thicker, larger plates, which can lead to inefficient designs and has negative effects on the inelastic deformation capacity [1]. A more recent approach outlines the desired yielding sequence of the brace and connection components to eliminate unwanted failure modes with the aim of maximizing the ductility of the connection while minimizing any premature damage. In this alternative, an $8t_p$ elliptical clearance is

suggested (Figure 1.3b) [16, 17], which results in smaller and more compact gusset plates while achieving with less local yielding in the adjacent columns and beams [18].

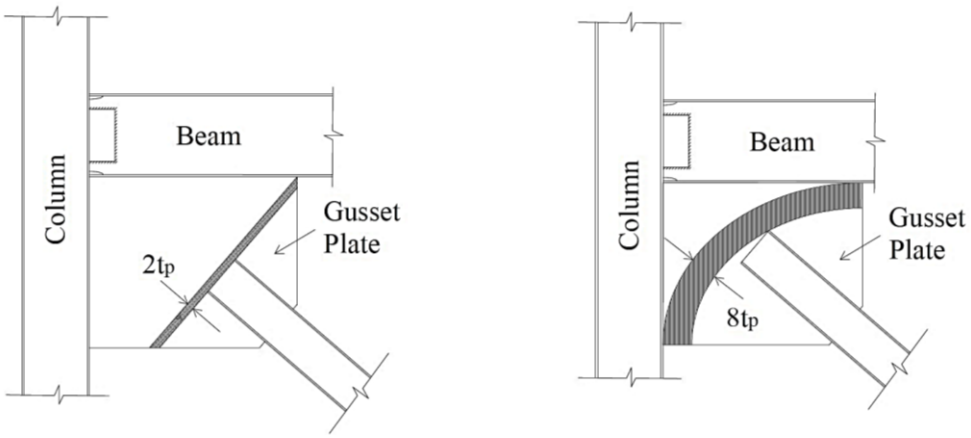

(a) (b)

Figure 1.3: Corner gusset plate connections. (a) Linear clearance. (b) Elliptical clearance.

While linear and elliptical clearance connection detailing methods both have their benefits, they have been shown to result in damage surrounding the gusset plate: in the adjacent beam and column for the linear 2tp design, and in the gusset-to-frame connection weld for the 8tp elliptical design [1, 12-16]. This study proposes a new method to achieve a more reliable yielding path through a heat softened zone. In this method, a pre-determined yield zone is created through reducing the local yield strength through heat treatment. The yielding path can be determined precisely, increasing the seismic performance of the gusset plate and connection in general. As a starting point, the elliptical yield line (Figure 1.4) is used for the heat treatment path.

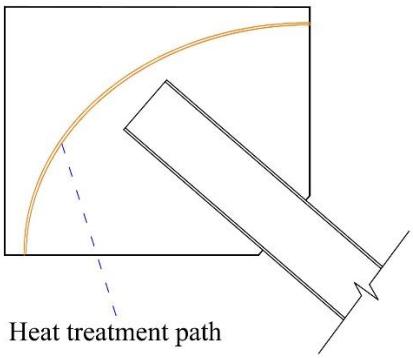

Figure 1.4: Heat treatment path

1.3. Braces

To dissipate energy and delay fracture and failure, global rather than local buckling is desired in braces. After repeated cycles and under higher drift ratios, local buckling develops, leading to deterioration and low-cycle fatigue. Increasing the ductility capacity and energy dissipation has been a topic of ongoing research. One alternative is to eliminate buckling, which has resulted in the development of buckling-resistant braces [19] and tension-only braces [20, 21]. An alternate approach is to accept brace buckling, but trying to enhance the buckling behavior.

The idea of using a combination of different steel types to design a multiphase bracing system was introduced by Shepherd in 1972 [22]. Shepherd used steel rods of different grades and showed that the proposed bracing system exhibited a varying stiffness based on the seismic intensity. More recently, Hsiao et al. [23] proposed naturally buckling steel braces (NBB), in which low-yield and high-strength steel channels are arranged in parallel with an initial eccentricity along the brace length. This eccentricity changes the buckling

behavior from a severe local buckling to smooth bending. This eccentricity also directs the buckling orientation to have higher strain in the low-strength steel section; as a result, the lower strength steel would experience an evenly-distributed plastic deformation while the high strength steel remains elastic. They showed that, within an appropriate design, NBB specimens yield at low drift ratios increasing energy dissipation and postpone buckling to higher drift ratios. Skalomenos et al. [24] proposed an induction-heated (IH) steel brace to achieve the same behavior of the NBB but with a single steel cross-section. The brace is composed of a normal strength steel tube in which one-half of the section is heat-treated longitudinally to increase the strength. Similar to NBB, an initial eccentricity was introduced. They showed that the new brace presents a higher tensile post-yielding stiffness and dissipates energy stably up to 2.0% story drift by delaying local buckling.

In a general-purpose application of steel tubes, which was focused on bending rather than axial loading, Siska et al. [25] performed carburization locally on steel tubes to enhance their bending behavior by delaying local buckling. By creating alternating high and low-strength rings, the behavior was shifted from local buckling to evenly-distributed deformation over the length of the specimen (Figure 1.5) which increased the maximum curvature. This improvement was obtained through changing the local deformation from inward kinking into distributed outward bulging in the low-strength rings.

Figure 1.5: Bending behavior of different tube specimens: Normal steel (top), fully carburized (middle), composite tube (bottom) [25]

Following the work by Siska et al., in this study, locally heat treated steel tube braces are proposed to study the effect of heat treatment on the brace performance. Three heat treatment configurations are investigated: ring-shaped, spiral, and cross-spiral paths (Figure 1.6).

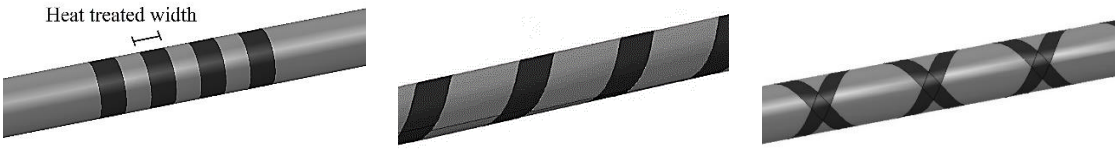

(a) (b) (c)

Figure 1.6: Heat treated paths. (a) Ring (b) Spiral (c) Cross-spiral

1.4. Objectives

The objectives of this research are:

- To study the efficiency of heat treatment in changing the mechanical behavior of structural steels.
- To propose a new design method for gusset plates which leads to smaller plates and less damage in the connection.
- To investigate heat treatment designs to achieve higher drift ratios in braces.

CHAPTER2: HEAT TREATMENT AND MATERIAL TESTING

To understand how various heat treatment protocols change common structural steel microstructures and the resulting strength and ductility, a series of coupon tests were conducted. First small samples were used to assess the effectiveness of the heat treating high and normal strength steels. Afterwards, larger coupons of high strength steels were treated and tensile and bending tests were conducted.

2.1. Microhardness Test

Small samples 10x10x6 mm of common structural steel for plates and sections, including normal strength steel A992 and A572 and high strength steel A514, were tested to identify appropriate heating and cooling protocols. The upper equilibrium austenitizing temperature, Ae3, can be estimated based on the chemical composition. As an example, the chemical composition of steel A514 is shown in Table 2.1. Based on the empirical formulas provided in the following [26-28], the austenitizing temperature was calculated to be 830°C.

Table 2.1: Chemical composition of A514.

Element	***Fe***	***C***	***Mn***	***Mo***	***Ti***	***Cr***	***Ni***	***Cu***	***P***	***S***	***Si***	***Al***
Result (%)	97.23	0.127	1.126	0.251	0.029	0.607	0.13	0.181	0.011	0.004	0.267	0.036

$$Ae_3(Celsius) = 910 - 203\sqrt{C} + 44.7Si - 15.2Ni + 31.5Mo + 30Mn + 11Cr + 20Cu - 700P - 400Al - 400Ti \quad (2.1)$$

$$Ae_3(Celsius) = 871 - 254.4\sqrt{C} + 51.7Si - 14.2Ni \quad (2.2)$$

$$Ae_3(Fahrenheit) = 1570 - 323C - 25Mn + 80Si - 3Cr - 32Ni \quad (2.3)$$

Based on this, a heating temperature of 830°C was used to guarantee austenite formation. The samples were held at the target temperature for 10 minutes and then cooled with different rates to 500°C, after which they were air cooled. One sample was air cooled and four other samples were cooled at 10 °C/min, 5 °C/min, 2 °C/min, and 1 °C/min. One sample was left completely untreated. The Vickers microhardness test was then performed by using a force of 200 gf to compare the effects of the different heat treatments. Figure 2.1 shows an indent measurement in the microhardness test. The tensile strength values, compared in Figure 2.2, were then estimated based on the microhardness tests.

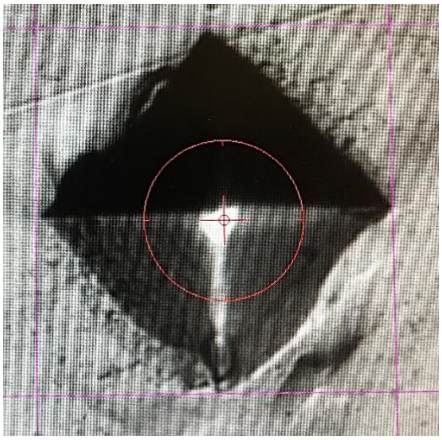

Figure 2.1: Indent measurement in Vicker's microhardness test performed on A992 steel

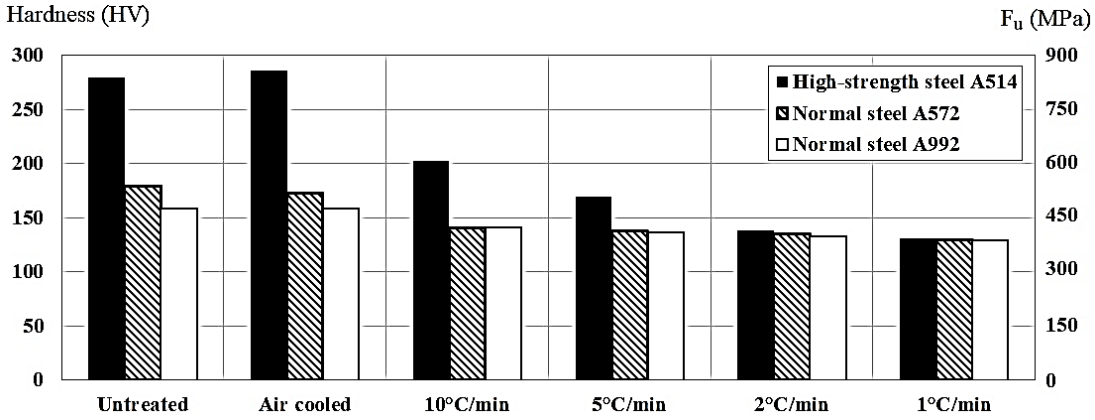

Figure 2.2: Microhardness test results for heat-treated steel materials.

For the high-strength A514 steel, the heat treatment with a cooling rate of 10 ºC/min reduced the tensile strength by 24%. This strength reduction was increased to 48% with a cooling rate of 2 ºC/min. However, there was no significant further reduction with 1 ºC/min. The A572 had a tensile strength reduction of 22% with a cooling rate of 10 ºC/min. However, there was no substantial reduction for slower cooling for this material. A992 showed the least strength reduction among all the steel materials. Its tensile strength was reduced by 11% and 18% when cooling at 10 ºC/min and 1 ºC/min, respectively. Larger strength reductions can be achieved for the higher strength steel (A514) because of the original microstructure. The as-received A514 has a high strength bainitic microstructure. When the steel is austenitized and slowly cooled to room temperature ferrite and pearlite are formed, leading to a softer microstructure (Figure 2.3). In contrast, the lower strength steels (A992) have a ferrite + pearlite microstructure to begin and there is a very limited opportunity to reduce the strength using the present heat-treatment approach. The strength of all the steels converged when the slowest cooling rate was used, as the microstructure of

all the steel materials transform into ferrite and pearlite when cooling is conducted sufficiently slowly.

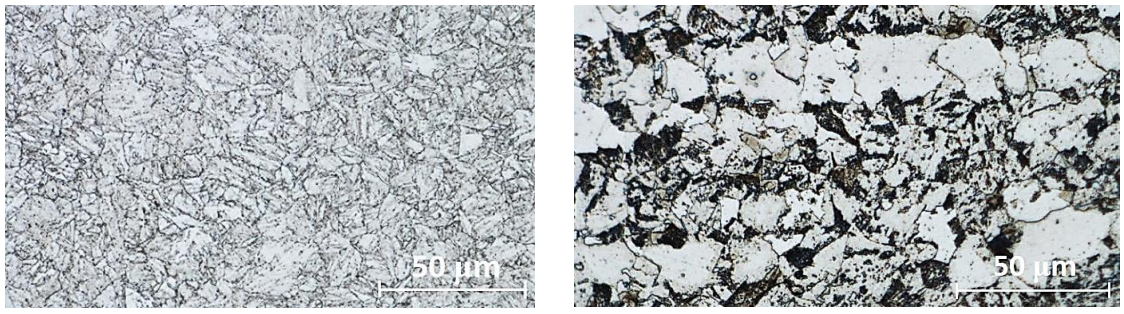

(a) (b)

Figure 2.3: Microscope images of steel A514 microstructure: (a) before heat treatment (b) after heat treatment with a cooling rate of 10 ºC/min.

Larger samples with the A514 steel with a 20 mm by 8 mm cross-section were then used to investigate the strength-weakening effect of localized heat treatment and the change in mechanical properties out of the heat treated zone through the length. The samples were heat treated locally in the middle 20 mm. The center was heated to the austenitizing temperature and held for 10 minutes before being cooled at either 10 ºC/min or 2 ºC/min. The temperature profiles after 10 minutes of heating, prior to cooling, were measured across the length of the samples; these temperatures along with the corresponding Vickers microhardness results measured after the cooling are shown in Figure 2.4.

The average temperature across the 20 mm heat-treated zone (HTZ) was 830 °C, which is sufficient for austenite transformation. At 20 mm away from the center, 10 mm outside the HTZ, the temperature dropped to 680°C, which is well below the austenitizing temperature. Therefore, beyond this point, there was no change in hardness due to heat treatment. Thus, the total width of the property-altered zone (PAZ) was roughly twice the

HTZ. The average reduction in microhardness for 2 ºC/min is 37% in the center, while it is 32% for 10 ºC/min. While these are similar reductions, the tests do show a correlation between the strength reduction and cooling rate. Thus, an appropriate cooling rate can be selected to obtain the required strength reduction.

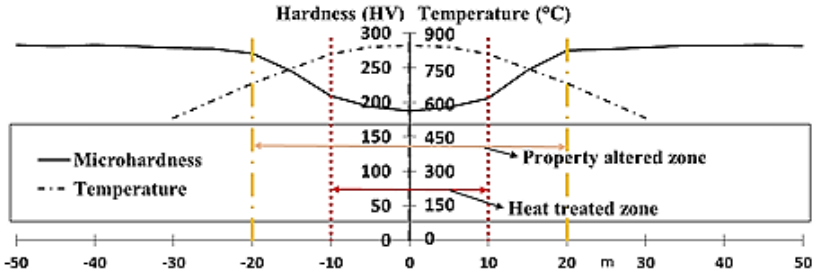

(a)

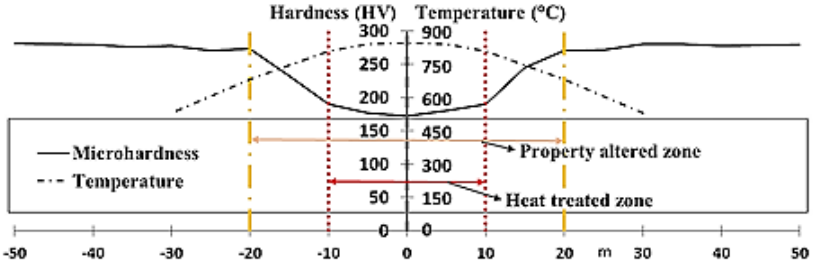

(b)

Figure 2.4: Microhardness and heating profiles for samples with cooling rates of: (a) 10°C/min. (b) 2 °C/min.

2.2. Tensile Test

Tensile tests were conducted for the two heat-treated coupons and one untreated coupon. The coupons dimensions are shown in Figure 2.5a. Similar heat treatment scenario with a maximum temperature of 830 °C, a holding time of 10 minutes, and a cooling rate of either 10 ºC/min or 2 ºC/min was performed in the middle 20 mm. The heating device is shown in Figure 2.5b and the heat treated sample is shown in Figure 2.5c. The results (Figure 2.6) shows that the strengths from the tensile tests are close to the estimates from the

microhardness test. In addition, the ductility capacity increased 64% for the 10 ºC/min specimen and 98% for the 2 ºC/min specimen.

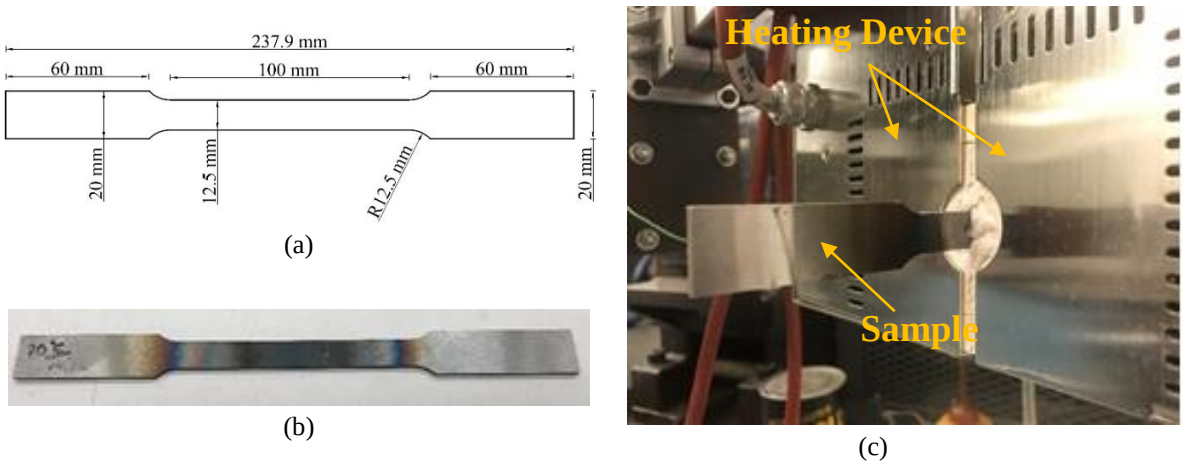

(a)

(b)

(c)

Figure 2.5: (a) Dimensions of the tensile sample. (b) Locally heat treated sample. (c) Heat treatment setup.

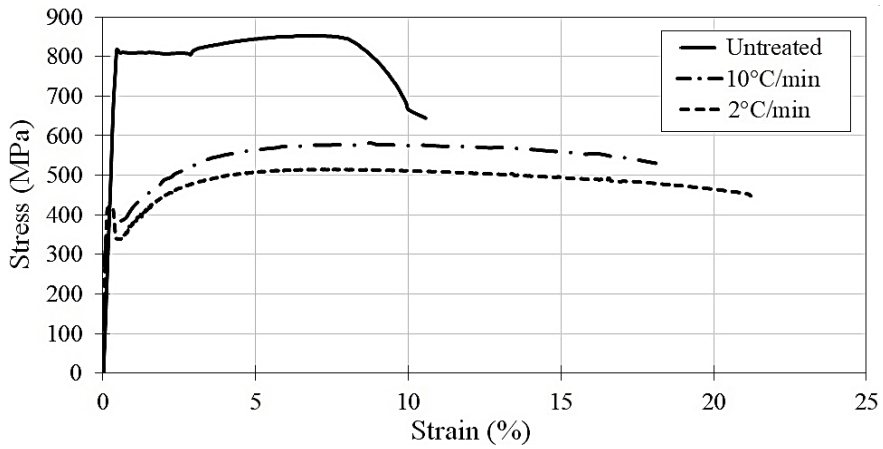

Figure 2.6: Stress-local strain curves of tensile samples.

Figure 2.7 shows that the heat treated samples successfully localized the strain to the PAZ, while in the untreated sample, the strain occurred along the length. The ability to localize the strain will be used to reinforce capacity design principles in the gusset plate design presented later.

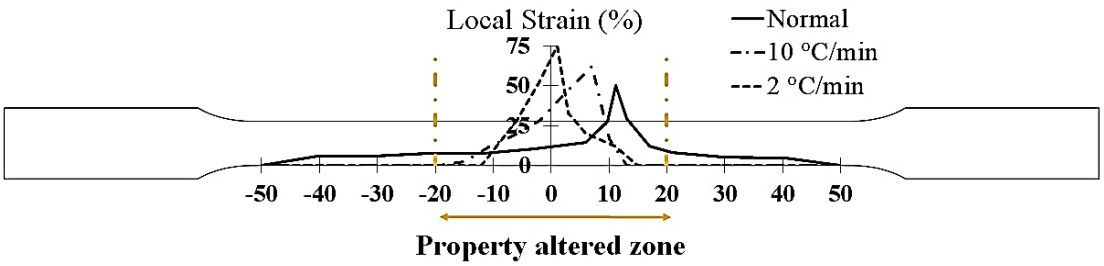

Figure 2.7: Local strain distribution over the length of the tensile samples.

2.3. V-bending Test

Bending tests were conducted on coupons with width of 19 mm, thickness of 2.7 mm, and length of 100 mm. The same heat treatment process was used as for the microhardness and tensile tests. Figure 2.8a shows the geometry of the V-bending test tool. The samples were bent to 60 degrees. Figure 2.8b shows the displacement-punch force curves for different samples; the punch force for the untreated sample reached 19 kN, while it reached 13 kN for the 10 ºC/min sample and 12 kN for the 2 ºC/min sample. No failure was observed for any of the specimen.

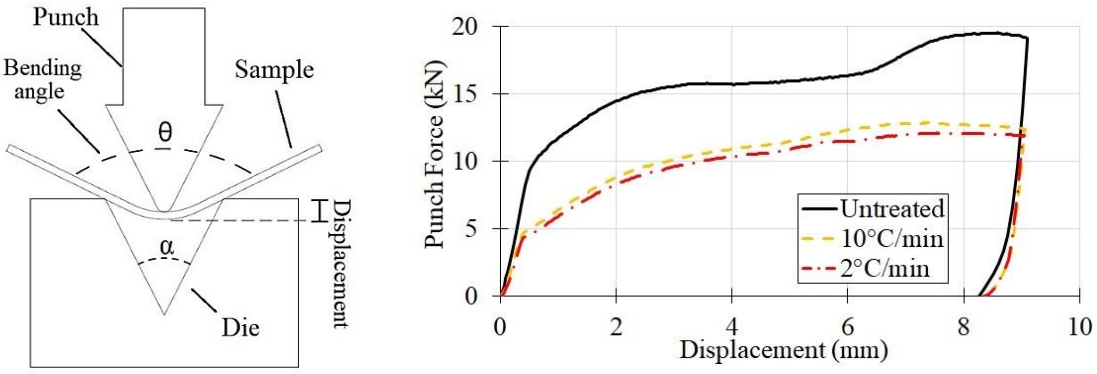

(a) (b)

Figure 2.8: V-bending test. (a) Geometry: α=30°, θ=60°. (b) Displacement-punch force curves of bending samples.

Figure 2.9 presents stereo-microscope images of the steel at the location of maximum curvature where the surface cracking seen is indicative of initiation of failure. There was substantial cracking on the surface of the untreated sample, with the largest crack 1.2 mm long. The 10 ºC/min sample had significantly less cracking, while the 2 ºC/min sample had no apparent cracks, indicating its increased ductility in bending.

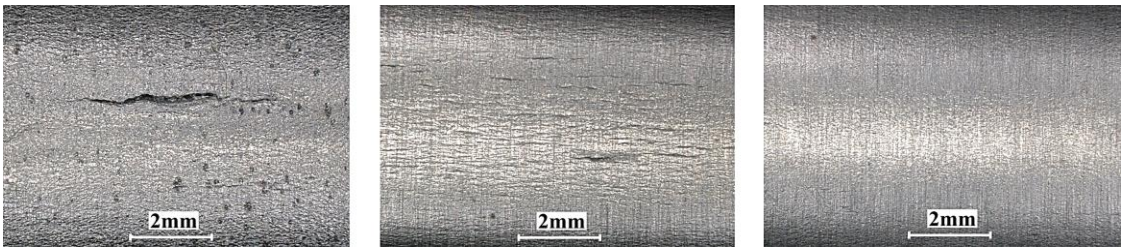

(a) (b) (c)

Figure 2.9: Optical microscope images of the middle of the bent samples. (a) Untreated. (b) 10 ºC/min. (c) 2 ºC/min.

CHAPTER3: HEAT TREATED GUSSET PLATES

To enhance the ductility of the gusset plate connection while maintaining a smaller size, a heat treatment method is proposed for CBF gusset plates. Starting with high strength steel, the yield strength of the plate is reduced locally in an elliptical heat treated path to enhance the rotational behavior of the gusset plate. A design methodology is developed, and using a ductile damage criterion, numerical models of normal, high strength, and heat treated high strength steel gusset plates are subjected to cyclic loading.

3.1. Design

3.1.1. Heat Treatment Configuration

In the proposed design method, heat treatment is used to reduce the yield strength to create a pre-determined yield zone on the gusset plate to enhance the inelastic rotational behavior of the gusset plate and minimize damage in the gusset-to-frame connection used under severe brace buckling. As shown in the material tests, high strength steel has the greatest capacity for strength reduction through heat treatment (Figure 2.2). Therefore, the heat treated gusset plate is designed out of high strength steel to use this difference between the strengths to create a distinct yield zone. The yield zone is taken as an elliptical-shape (Figure 3.1) to minimize the gusset plate dimensions. Design with elliptical yield zone calls for an $8t_p$ zone width [29]. From the results of the material tests, a PAZ half of the HTZ is assumed; thus, the HTZ width of the heat treated zone is taken as $4t_p$ with a PAZ of $2t_p$ in each side. As the width of the PAZ will depend on the thickness of the plate and heat treatment conditions, the width of HTZ and PAZ can be adjusted to remain $8t_p$.

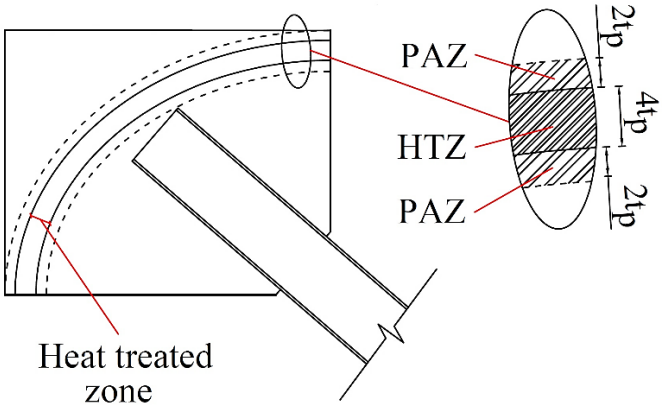

Figure 3.1: Heat treated gusset plate.

3.1.2. Failure Mechanisms

There is a variety of failure mechanisms that must be considered during connection design in CBFs (Figure 3.2a). Balanced design procedure proposes a hierarchy to consider possible failure mechanisms in designing a CBF frame [29]. In this procedure, the resistance of each failure mechanism is calculated so that desirable failure modes are prioritized, ensuring brace yielding and buckling, and increasing inelastic deformation capacity of the connection. For heat treated gusset plates, there are additional failure mechanisms that should be considered. The most critical one is the tension yielding across the lower strength heat treated zone. This critical area is defined as part of the HTZ which is located between the two lines making a 30-degree angle with the brace, similar to Whitmore width (Figure 3.2b).

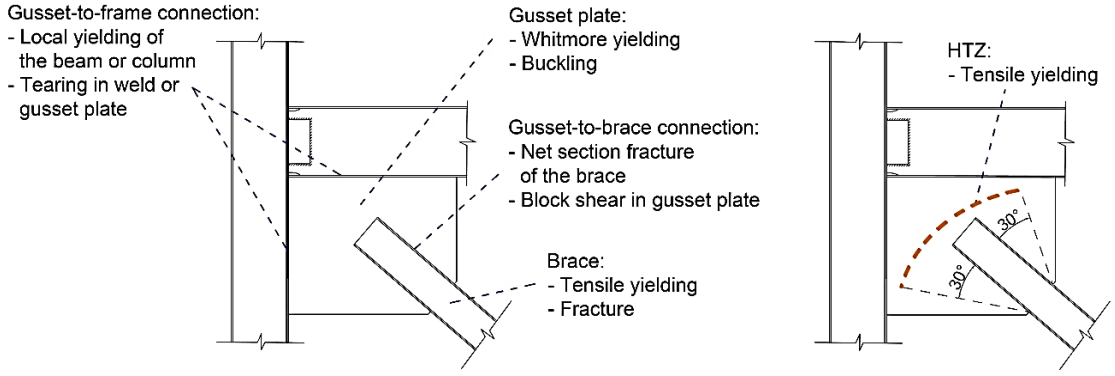

Figure 3.2: (a) Failure modes for gusset plates (after [16]). (b) Additional failure modes for a heat treated CBF connection.

3.1.3. Gusset Plate Design

In determining the thickness of the heat treated gusset plate, the tensile yielding capacity of the heat treated path should be greater than probable tensile force of the brace:

$$R_{yH}F_{yH}L_H t_H > R_{yb}F_{yb}A_g \tag{3.1}$$

In above equation, R_{yb} and R_{yH} are the ratio of the expected to specified yield stress of the brace steel and heat treated gusset plate, respectively. F_{yb} is the yield stress of the brace, and F_{yH} is the yield stress for the heat treated portion of the gusset plate. L_H is the length of the critical tensile yielding area of the HTZ (Figure 3.2b). A_g is the gross section area of the brace, and t_H is the thickness of the gusset plate. Based on Eq. (3.1), the thickness of the gusset plate t_H is chosen. The thickness is predominantly dependent on the yield stress of the heat treated zone F_{yH} which is determined through the heat treatment process cooling rate.

A set of pre-designed one-story one-bay braced frame systems were chosen based on different observed failure mechanisms, including gusset plate tearing and brace fracture, and different configurations including brace angle and section properties. The first two cases were chosen from the tests conducted by Powell [30] (Figure 3.3). The experimentally observed failure mechanisms of these CBFs were gusset plate tearing and weld tearing near the gusset-to-frame connection. Case 1 has a tapered gusset plate with a HSS-section brace and a moment-free beam-to-column connection. Case 2 has a rectangular gusset plate with a W-section brace and a rigid beam-to-column connection. In both cases, an $8t_p$ elliptical clearance was included for the out-of-plane rotation.

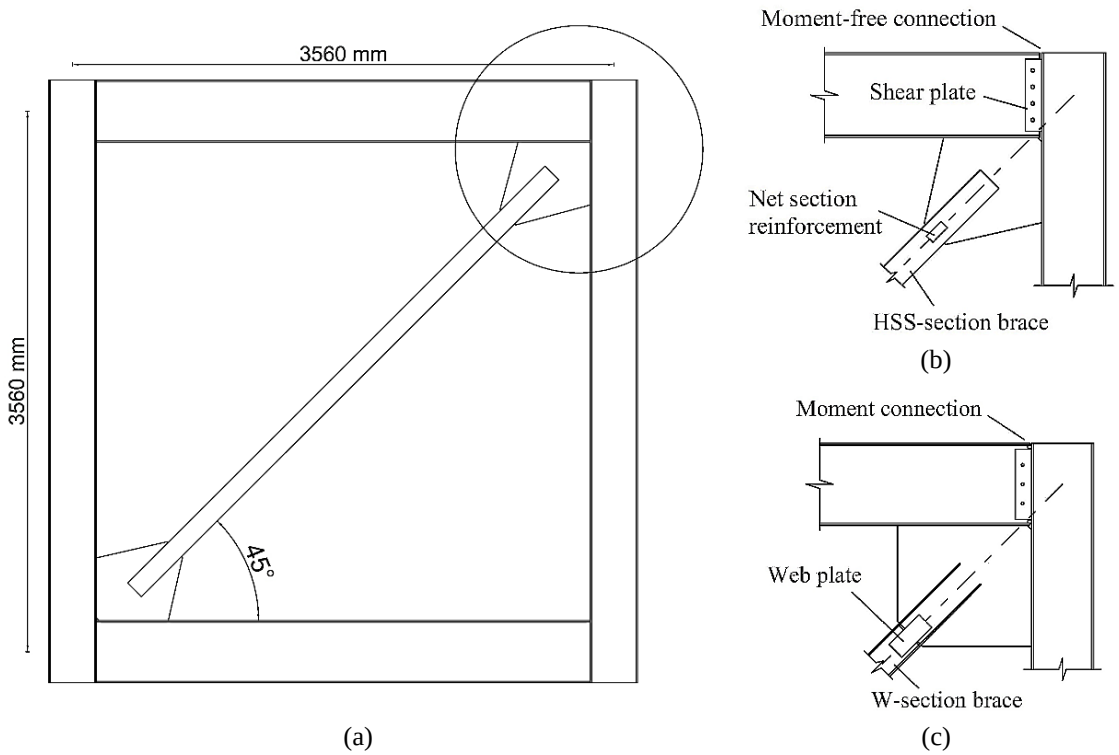

Figure 3.3: (a) The CBF configuration for Cases 1 and 2. (b) Details of Case 1. (c) Details of Case 2

The combinations of beams, columns, and brace sizes used for Cases 3,4, and 5 were chosen from previous numerical studies [29, 31, 32], respectively. For computational efficiency, only the end parts of the beam and column were considered in the modeling for these three cases (Figure 3.4). Gusset plates were designed for each case from normal steel A572, high strength steel A514, and heat treated high strength steel. An $8t_p$ elliptical clearance was considered for all plates. A design example is provided in Appendix A. Table 3.1 shows the section profiles and dimensions. As the result of the higher strength, using A514 reduces gusset plate dimensions, with plates that are 55% of the volume of the normal strength steel on average. This can save on the cost of material, labour, erection, and transportation [6]. The heat-treated gusset plates are thicker than the untreated ones because of concern of tensile yielding in the heat treated zone; however, they are still around 25% smaller than the normal plates.

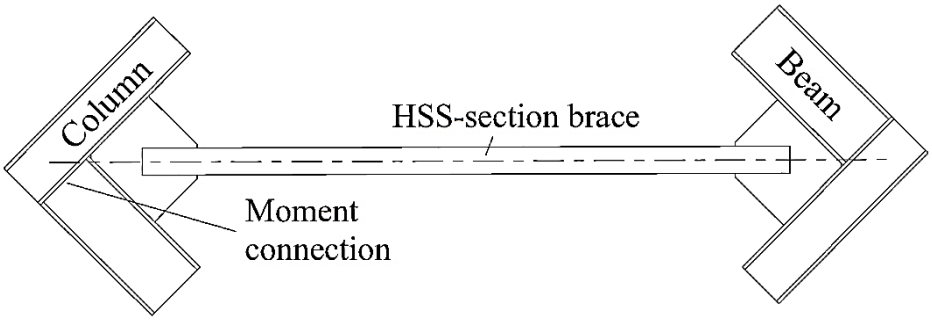

Figure 3.4: The CBF configuration for Cases 3 to 5.

Table 3.1: Structural sections and steel types used for the elements.

Case	Specimen	Brace		Beam and Column	Gusset plate	
		Angle degrees	Section		Material	Size (mm)
1	N1 H1 HT1	45°	HSS127x9.5	W410x67 W310x107	A572 A514 HT A514	455x413x10 380x328x7 420x358x8
2	N2 H2 HT2	45°	W150x37	W410x67 W310x107	A572 A514 HT A514	556x508x10 526x478x6 540x490x8
3	N3 H3 HT3	45°	HSS178x9.5	W530x101 W310x158	A572 A514 HT A514	715x610x17 653x548x10 688x583x14
4	N4 H4 HT4	40°	HSS203x13	W610x241 W360x551	A572 A514 HT A514	1068x792x18 985x723x10 1026x758x14
5	N5 H5 HT5	55°	HSS178x13	W610x113 W360x216	A572 A514 HT A514	704x910x18 649x834x10 672x878x14

3.2. Numerical Modelling

3.2.1 General Description

To evaluate the performance of the gusset plates and bracing system, nonlinear finite element analysis with ABAQUS was used [33]. The models and boundary conditions are illustrated in Figure 3.5. For Case 1 and 2 (Figure 3.5a), two axial loads, each equal to1557 kN, was applied to the columns to model gravity loads as done in the experiment [30]. Four-node quadrilateral shell elements (S4R) with five integration points through the thickness were used to model all elements. A high mesh density was used for the gusset plate, gusset-to-connection zone, and center portion of the brace to capture the bending and damage of the gusset plate and gusset plate connection as well as brace buckling. Coarser meshes were used where elastic behavior was expected. An initial imperfection using a

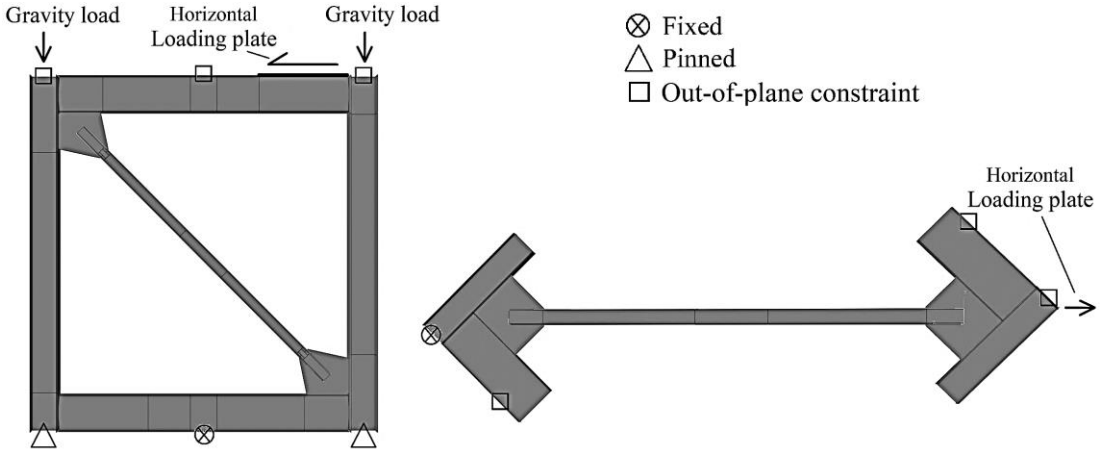

Figure 3.5: Abaqus models and boundary conditions. (a) Cases 1 and 2. (b) Cases 3 to 5.

combination of the 1st and 2nd buckling modes with amplitudes of *B*/1000 and *B*/2000, respectively, was used, where *B* is the brace length between the working points. A nonlinear combined isotropic-kinematic hardening material model was used in the inelastic analysis.

3.2.2. Ductile Damage Criterion

A ductile damage criterion was included in the model to predict the onset of damage and simulate fracture from low cycle fatigue [34]. The ductile criterion model predicts the onset of damage due to nucleation, growth, and coalescence of voids. Damage starts to initiate when the damage initiation parameter, ω_D, is equal to 1

$$\omega_D = \int \frac{d\bar{\varepsilon}^{pl}}{\bar{\varepsilon}^{pl}{}_D\left(T, \dot{\bar{\varepsilon}}^{pl}\right)} = 1 \tag{4.1}$$

In this equation, T is the stress triaxiality, $\bar{\varepsilon}^{pl}$ is the equivalent plastic strain, and $\bar{\varepsilon}^{pl}{}_D$ is the equivalent plastic strain at the onset of damage, which is a function of stress triaxiality and the equivalent plastic strain rate, $\dot{\bar{\varepsilon}}^{pl}$. Stress triaxiality is $T = -\frac{p}{q}$, in which p is the

pressure stress and q is the Mises equivalent stress. Figure 3.6 presents the stress triaxiality values for some general cases of stress distribution in two-dimensional elements.

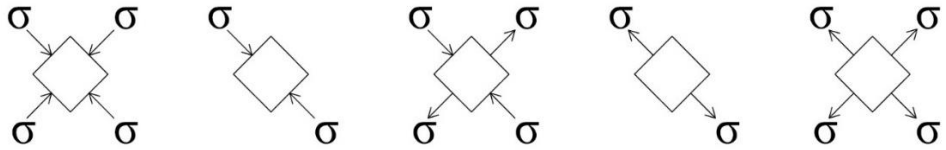

T=-0.66 T=-0.33 T=0 T=0.33 T=0.66

Figure 3.6: Stress triaxiality for general cases of stress distribution in two dimensions.

Significant research has been conducted to construct theoretical and empirical models to develop relationship between equivalent plastic strain and stress triaxiality and capture ductile fracture [35]. In this work, the void growth model, developed by Rice et al. [36], is used for the equivalent plastic strain (EPS) at damage as

$$\bar{\varepsilon}^{pl}(T) = \eta e^{-\beta T} \tag{4.2}$$

Where η and β are material constants, which are determined and calibrated through circumferential-notched tensile test (CNT). Saykin et al. [36] found η and β to be 1.8 and 1.56 for A572, 1.91 and 1.85 for A992, and 1.85 and 1.75 for A514. After damage initiation, the degradation of the material is modeled using a scalar damage variable, D, where

$$D = \int \frac{L\sigma_y}{G_f} d\bar{\varepsilon}^{pl} \tag{4.3}$$

where L is the mesh characteristic length, and G_f is the fracture energy found by

$$G_f = \int \sigma_y \, d\bar{u}^{pl} = \int L\sigma_y \, d\bar{\varepsilon}^{pl} \tag{4.4}$$

And

$$\dot{\bar{u}}^{pl} = L\dot{\bar{\varepsilon}}^{pl} \tag{4.5}$$

The fracture energy is the area under the stress deformation diagram (Figure 3.7)

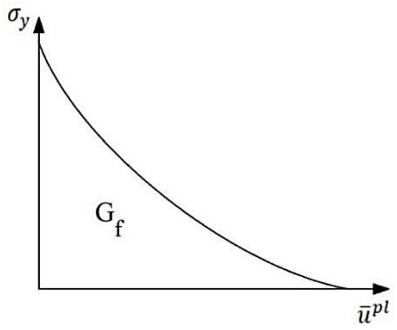

Figure 3.7: Fracture energy

As inelastic deformation increases in a mesh element, damage initiation and material degradation occur; when *D* is almost 1 the element is assumed to have failed and is deleted resulting in cracking and subsequently tearing. A schematic of ductile damage modeling is shown in Figure 3.8. In the figure, $\sigma_{D=0}$ is the yield stress at the onset of damage.

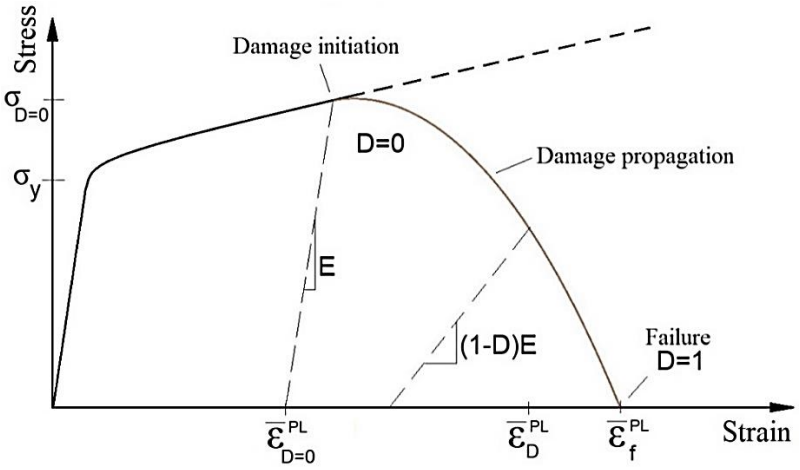

Figure 3.8: Stress-strain curve including degradation of material.

3.2.3. Verification

To verify that the finite element models can capture global brace buckling behavior and predict the brace fracture, an HSS brace with gusset plates tested by Fell [38] which experienced brace fracture was simulated. An initial imperfection using a combination of the 1st and 2nd buckling modes with amplitudes of *B*/1000 and *B*/2000, respectively, was used, where *B* is the brace length between the working points. The ductile damage criterion which was explained in the previous section was implemented. The axial force-drift curves of the experiment and numerical model are shown in Figure 3.9. The model can represent the hysteretic behavior and predict the onset of damage and failure of the brace.

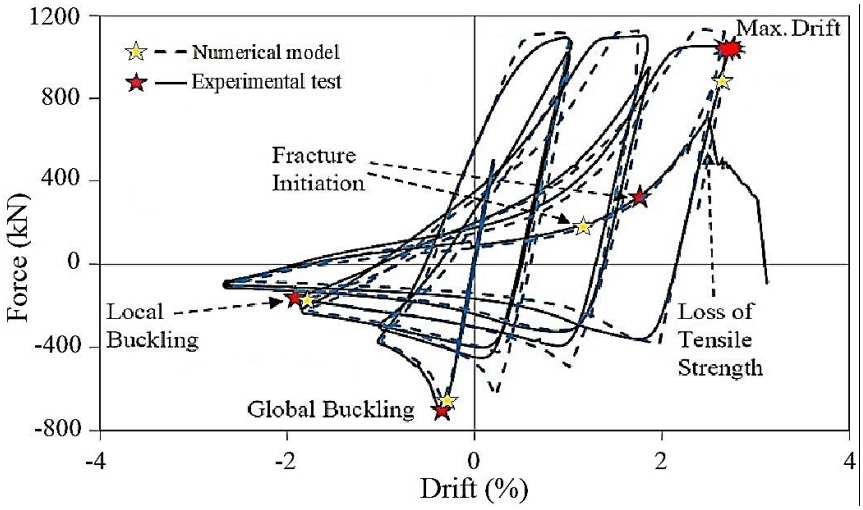

Figure 3.9: Validation of numerical model against experimental results [35] for cyclic testing of a brace.

3.3. Analysis Results

Cyclic displacement-control protocols were used for the analysis. For Cases 1 and 2, the same loading protocol as the experimental testing was used in the analysis (Figure 3.10a). For the other specimens, the loading protocol from ATC-24 [39] was used (Figure 3.10b).

The cycle amplitudes were modified according to the brace buckling displacement to ensure that both elastic and inelastic cycles were captured. The displacement loading was continued up to failure.

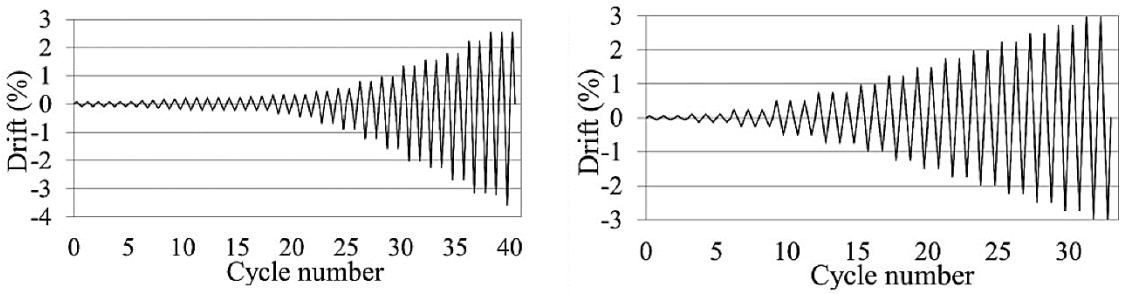

(a) (b)

Figure 3.10: Loading protocols for: (a) Cases 1 and 2, (b) Cases 3 to 5.

3.3.1. Cases 1 and 2

For Cases 1 and 2, the numerical model using the normal strength gusset plates (Specimen N1 and N2), predicted a failure mode of gusset plate cracking and tearing near the gusset-to-frame connection, which is in agreement with the experimental results [29]. Tearing here is defined as when a crack of length of $4t_p$ is reached (Figure 3.11). To study the effect of using high strength steel and heat treatment on gusset plates, Specimens N, H, and HT with normal steel, high strength steel and heat treated high strength steel, respectively (Table 3.1), were modeled and subjected to the same loading protocols. The axial load versus story drift curves for the specimens of Cases 1 and 2 up to their maximum achieved drift ratios are presented in Figure 3.12.

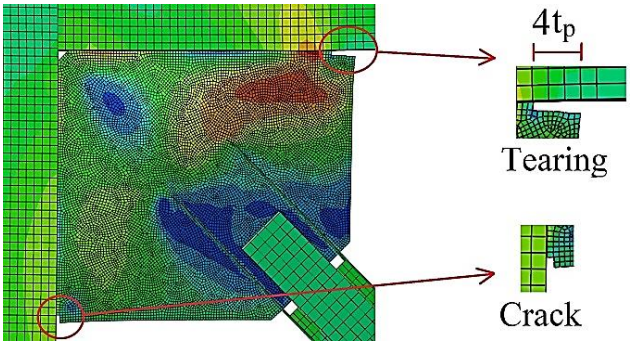

Figure 3.11: Cracking in gusset plates near gusset-to-frame connection in Case 2.

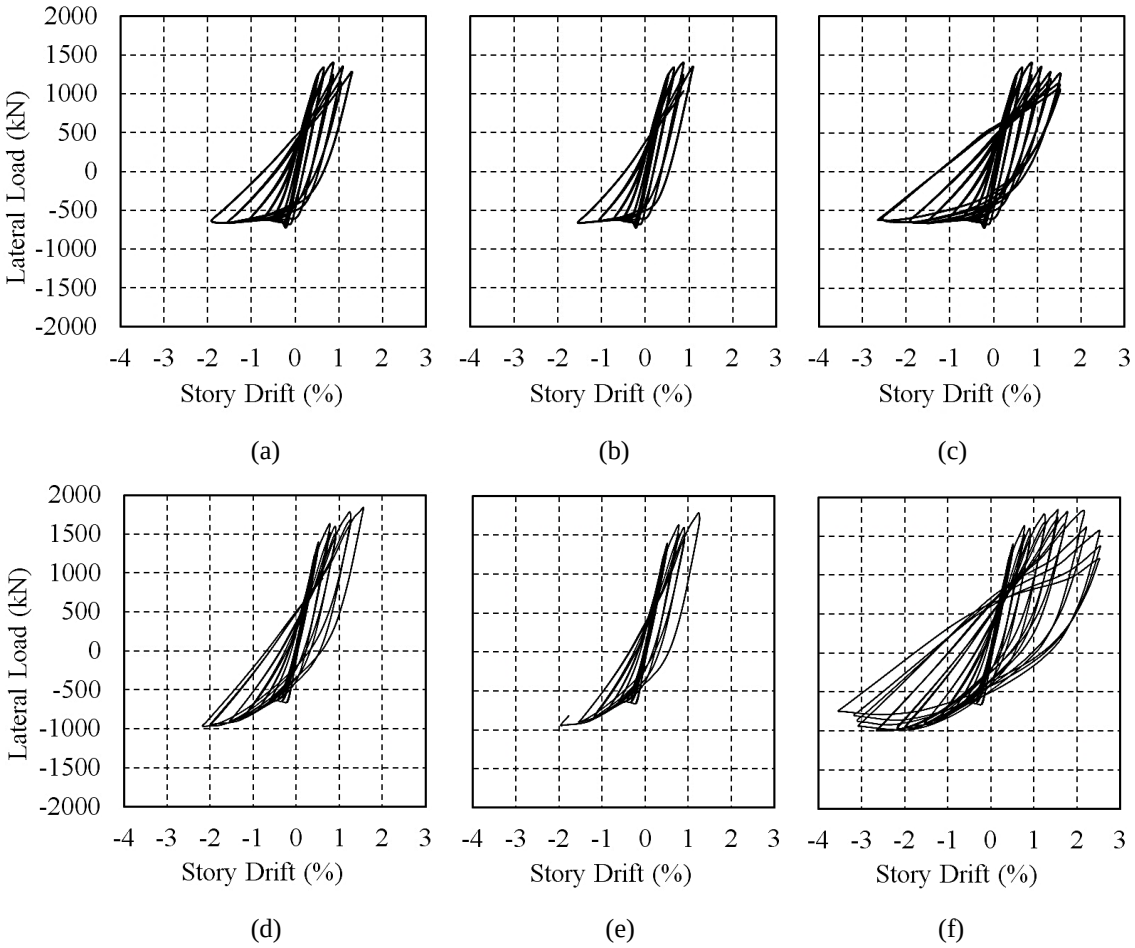

Figure 3.12: Hysteretic curves of: (a) Specimen N1. (b) Specimen H1. (c) Specimen HT1. (d) Specimen N2. (e) Specimen H2. (f) Specimen HT2.

The behavior of the gusset plates during the cyclic loading are summarized in Table 3.2. For Case 1, the numerical results show that the first yielding in Specimen N1 gusset plate occurred at a drift of 0.22% at the gusset-to-beam region; initiation of cracking occurred at a story drift of -1.56%, with negative sign representing compression, and tearing developed at a story drift of -2%. For Specimen H1, first yield occurred at the same location as N1 at a drift ratio of 0.33%; crack initiation occurred at the second cycle of a story drift of -1.12%, and tearing occurred at a story drift of -1.56%. Thus, for the high strength gusset plate, the first yielding occurred at a higher drift ratio than for the normal strength plate; however, the crack initiation and failure occurred at lower drift ratios as the result of repeated local buckling of the high strength gusset plate due to the frame action in high drift ratios. For the heat treated specimen, HT1, the first yielding occurred in the heat treated zone (away from the gusset-to-beam connection) at a drift of 0.44%. Yielding then spread to the gusset-to-beam connection at a drift 0.54%. The first crack occurred in the gusset-to- beam connection under the -2.00% drift cycle, and tearing occurred in the -2.68% cycle. The maximum drift ratio of the heat treated specimen increased by 34% compared to Specimen N1 and increased 72% compared to Specimen H1. Figure 3.13 shows the propagated crack in Case 1 specimens up to a 1.56% drift. Similar results were seen for Case 2. Tearing in Specimen N2 occurred at a drift of -2.23%. For Specimens H2 and HT2, these drift ratios were -2.00% and -3.12%, respectively. Again, the heat treated specimen HT2 reached the highest drift ratio, roughly 40% and 56% more than the maximum drift ratio of Specimen N2 and H2, respectively.

Table 3.2: Analysis results of the gusset plate and CBF performance for Cases 1 and 2.

Specimen	Drift levels (%)				
	First yielding in gusset plate	Crack initiation		Tearing	
		Cycle	Cycle Amplitude	Cycle	Cycle Amplitude
N1	0.22	1st	-1.56	1st	-2.00
H1	0.45	2nd	-1.12	1st	-1.56
HT1	0.44	2nd	-2.00	2nd	-2.68
N2	0.27	2nd	-1.56	1st	-2.23
H2	0.33	2nd	-1.56	1st	-2.00
HT2	0.54	1st	-2.68	1st	-3.12

The EPS $\bar{\varepsilon}^{pl}$ is one of the determining factors in damage initiation and propagation (Eqs 4.2 to 4.4). In Figure 3.14, the maximum values of EPS, recorded at the end of the cyclic loading, of the normal and heat treated specimens of Case 2, N2 and HT2, at the connections to the beam and column are shown. The largest EPS values are located near

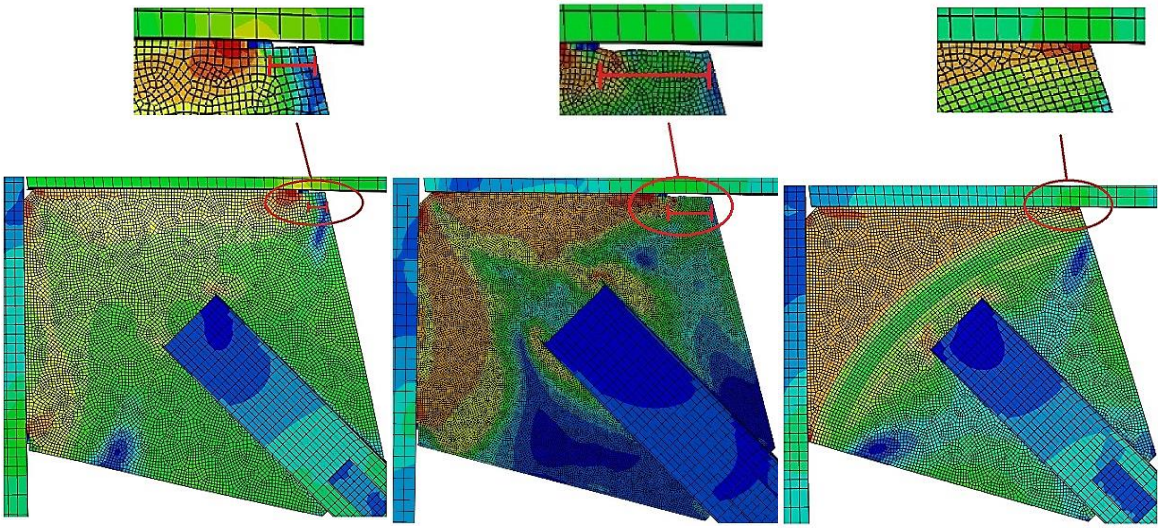

(a) (b) (c)

Figure 3.13: Crack length in Case 1 gusset plate: (a) Specimen N1, (b) Specimen H1, (c) Specimen HT1.

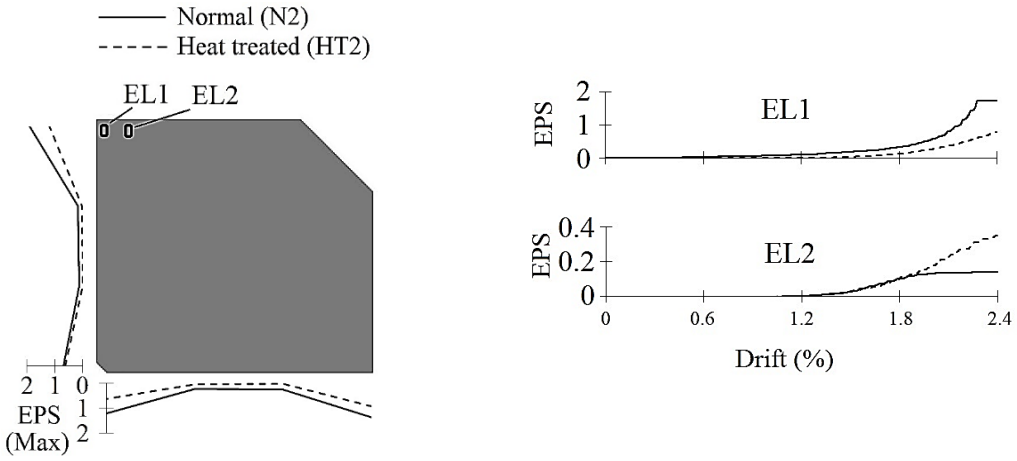

(a) (b)

Figure 3.14: Equivalent plastic strain in normal and heat treated high strength gusset plates of Case 2: (a) Maximum values along the connection edge. (b) Near the connection (EL1) and in the heat treated zone (EL2).

the corner of the gusset plate edges, which shows the location of damage initiation and tearing (Figure 3.14a). The heat treatment reduced the maximum EPS values by up to 70%. In Figure 3.14b, the EPS values for two mesh elements were recorded: one near the connection (EL1), and the other one away from the connection and in the heat treated zone (EL2). Heat treatment reduced the EPS values at EL1 by almost 70% and simultaneously increased in the EPS in EL2. This shows that heat treatment can move the plastic deformation from the connection towards the heat treated zone.

3.3.2. Cases 3 to 5

Cases 3 to 5 were used to compare the behavior of the various gusset plate designs when the failure mode with a normal strength gusset plate is brace fracture rather than gusset plate or weld tearing. The hysteretic behavior of the braces with normal gusset plates (Specimens N3, N4, and N5) are shown in Figure 3.15. Again, the high strength and heat

treated gusset plates result in similar in shape and in peak drift capacity as the hysteresis curves are dependent mainly on brace behavior rather than gusset plate material and geometry. Extensive inelastic deformation at the connection can result in premature failure [7]. Hence, shifting of the plastic zone away from the connection, or reducing plastic deformation in the connection area near welding, can enhance the reliability of achieving the desired gusset plate connection performance. In order to study the inelastic demands at the gusset plate connection, the stress-strain curves of an element at the connection (shown in Figure 3.16a) were recorded for the various designs (Figure 3.16), all cycled to the same drift ratio.

For Specimen N3, significant yielding can be observed; by using high strength steel (H3) ultimate strain was reduced by 15%. However, for the heat treated gusset plate HT3, the element experienced only a small amount of plasticity, with a reduction in strain of 68% from N3. Similarly, the heat treated specimens HT4 and HT5 showed the lowest inelastic deformation for Cases 4 and 5, while the high strength gusset plates experienced inelastic

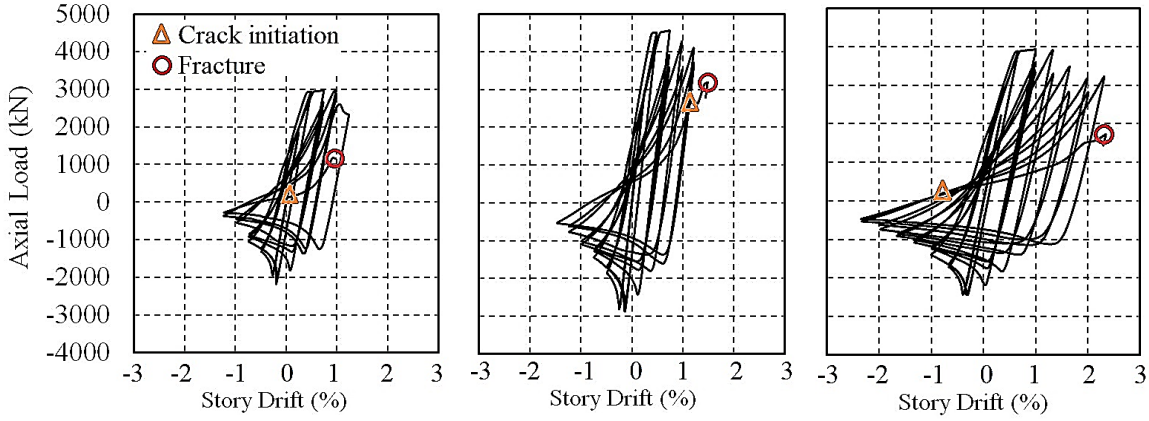

Figure 3.15: Hysteretic curves of: (a) Specimen N3, (b) Specimen N4, (c) Specimen N5.

deformations on the same order as the normal plates. Thus, while high strength steel offers the smallest gusset plate design, it does not provide enhanced cyclic behavior unless heat treatment is used.

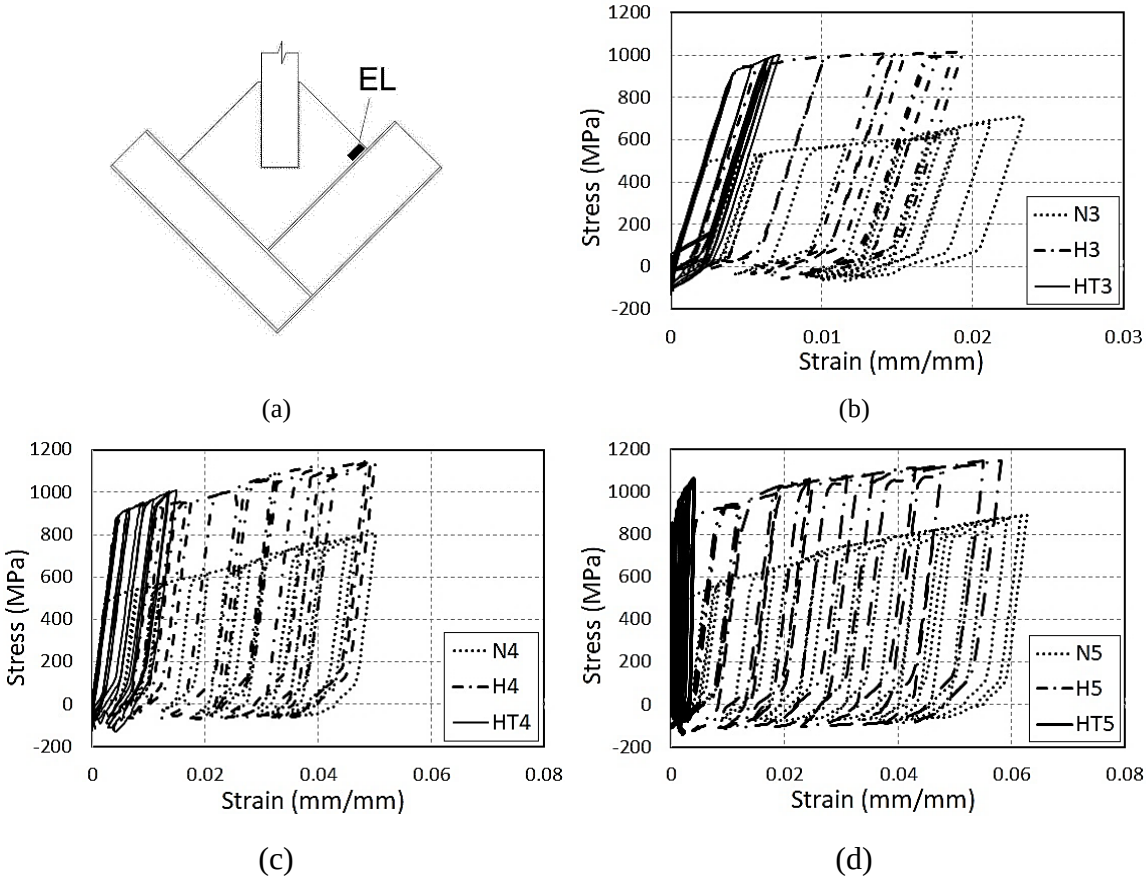

Figure 3.16: Hysteretic curves of the gusset plate edge element: (a) Element location, (b) Case 3, (c) Case 4, (d) Case 5.

CHAPTER4: HEAT TREATMENT ON BRACES

Repeated brace buckling results in premature fracture in the middle length, reducing the CBF ductility when compared to MRFs. To address this issue, in this chapter, heat treatment is used this time to increase the yield and tensile strength locally to create high-strength ring-shape, spiral-shape, and cross-spiral paths on the braces. Starting with normal strength steel tube, high strength rings and spirals are created on braces to enhance their hysteretic performance. Higher strengths are achieved by quick quenching the steel after heating, creating bainite and martensite (Figure 1.2b), which increases the yield and tensile strength of the steel, but at the same time, reduces the ductility. To increase the temperature, induction heating or welding lasers could be used. Both methods are finely controllable source to produce high temperature heat for variable configurations [28, 40]. Multiple heat treatment configurations are proposed for the brace, and for each configuration, various heat treated widths are investigated in the numerical modeling to study their effects in terms of maximum axial forces and drift ratios achieved through cyclic loading.

4.1. Design

4.1.1. Material properties

The properties of the heat treated brace used in this study are taken from those found experimentally by Skalomenos et al. [24] who used induction heating on normal strength steel tubes by heating the steel to 1000°C and then cooling rapidly by water. The mechanical properties of the steel tube before and after the heat treatment are provided in Table 4.1. It is seen that, after heat treatment, the yield strength and the ultimate strength

increased by 90% and 69%, respectively. However, plastic elongation reduced by 68%, which can be considered a disadvantage of strengthening.

Table 4.1: Mechanical properties of the coupons before and after heat treatment [23].

Material	Yield strength (MPa)	Ultimate strength (MPa)	Elongation (%)
Before heat treatment	354	460	21.7
After heat treatment	671	778	6.9

4.1.2. Local buckling

Local buckling appears in tubes in a wave form (Figure 4.1), with a wavelength which depends on the diameter (D) and thickness (t) of the section. Siska et al. showed that the wavelength of local buckling λ (wrinkling) of a number of tubular section is proportional to two and half times the square root of D times t [25]. In this study, to extend this to structural sections commonly used in construction, a number of circular and square hollow structural sections (HSS) with different diameter or width (W) to thickness ratios ranging from 10 to 46 were modeled numerically, and the local buckling mode shapes are studied. The wavelengths for common sections are shown in Table 4.2. and Table 4.3. Based on the wavelength found numerically, the local buckling wavelength can be approximated by $\lambda = 2.61\sqrt{Dt}$ for circular HSS sections and $\lambda = 1.6W$ for square HSS sections.

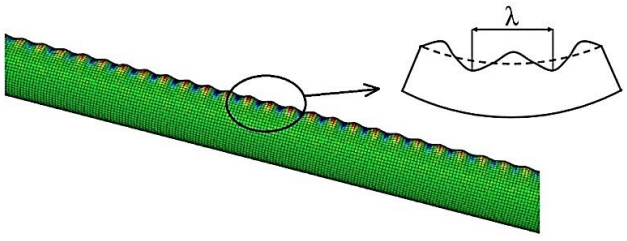

Figure 4.1: Local buckling wavelength.

Table 4.2: Local buckling wavelength for circular HSS sections

Section (HSS)	Diameter (mm)	Thickness (mm)	D/t	λ (mm) (Abaqus)	λ (mm) (2.61√(Dt))	Error (%)
127X3.2	127	3.2	39.69	57.31	52.62	8.19
127X4.8	127	4.8	26.46	66.6	64.44	3.24
127X6.4	127	6.4	19.84	74.34	74.41	0.09
127X8	127	8.0	15.88	81.57	83.19	1.99
127X9.5	127	9.5	13.37	86.73	90.66	4.53
127X13	127	12.7	9.77	97.06	106.05	9.26
178X4.8	178	4.8	37.08	82.49	76.29	7.52
178X6.4	178	6.4	27.81	89.72	88.09	1.81
178X8	178	8.0	22.25	99.85	98.49	1.36
178X9.5	178	9.5	18.74	106.37	107.33	0.90
178X13	178	12.7	13.69	121.56	125.55	3.28
219X4.8	219	4.8	45.63	93.48	84.62	9.48
219X6.4	219	6.4	34.22	104.16	97.71	6.19
219X9.5	219	9.5	23.05	122.85	119.05	3.09
219X13	219	12.7	16.85	135.32	139.26	2.91
219X16	219	15.9	13.69	149.56	154.50	3.30

Table 4.3: Local buckling wavelength for square HSS sections

Section (HSS)	Width (mm)	Thickness (mm)	W/t	λ (mm) (Abaqus)	λ/W	Error* (%)
127X4.8	127	4.8	26.46	215	1.693	9.22
127X6.4	127	6.4	19.84	199.5	1.571	1.35
127X8	127	8.0	15.88	193.6	1.524	-1.65
127X9.5	127	9.5	13.37	191.28	1.506	-2.83
127X13	127	12.7	9.77	183.21	1.443	-6.93
178X4.8	178	4.8	37.08	283.35	1.592	2.70
178X6.4	178	6.4	27.81	281.17	1.580	1.91
178X8	178	8.0	22.25	278.99	1.567	1.12
178X9.5	178	9.5	18.74	275.5	1.548	-0.14
178X13	178	12.7	13.69	266.78	1.499	-3.31
178X16	178	15.9	11.13	259.37	1.457	-5.99
254X6.4	254	6.4	39.69	407.22	1.603	3.43
254X8	254	8.0	31.75	401.21	1.580	1.91
254X9.5	254	9.5	26.74	401.19	1.579	1.90
254X13	254	12.7	19.54	393.1	1.548	-0.15
254X16	254	15.9	15.88	386.88	1.523	-1.73

* Error is defined as the difference between Abaqus results and $\lambda = 1.6W$.

4.1.3. Material combination

Siska et al. [25] showed that for sections with D/t = 20, altering the material property in ring widths between 0.5λ to 1.5λ enhanced the bending behavior of the section. Using the same approach, three proposed braces are investigated which are composed of normal strength structural tube sections heat treated in ring-shaped, spiral, and cross-spiral paths. Table 4.4 and Figure 4.2 show the heat treated brace designs.

Table 4.4: Heat treatment cases of Abaqus models.

Specimen	Heat treatment	Heat treated width	Untreated width
N	Normal (untreated)	-	Full length
HT	Fully heat treated	Full length	-
R1	Ring	1.5λ	1.5λ
R2	Ring	1.0λ	1.0λ
R3	Ring	0.75λ	0.75λ
R4	Ring	0.5λ	0.5λ
S1	Spiral	1.0λ	2.0λ
S2	Spiral	1.0λ	1.0λ
S3	Spiral	0.5λ	1.0λ
S4	Spiral	0.5λ	0.5λ
CS1	Cross Spiral	0.5λ	1.0λ
CS2	Cross Spiral	0.5λ	2.0λ

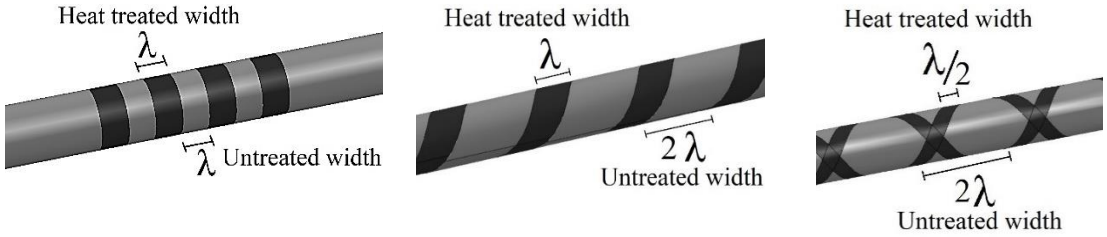

(a) (b) (c)

Figure 4.2: Heat treated braces: (a) Specimen R4 (b) Specimen S1 (c) CS2

4.2. Numerical Modelling

Steel tube braces with gusset plate connections at the ends were designed using one-third scale based on the balanced design procedure. Both the gusset plate and the brace are made of normal strength steel. Tubular hollow structural steel section with an outer diameter of 64 mm and a thickness of 3.2 mm was used for the brace. The dimensions of the brace and the gusset plates are shown in Figure 4.3. A $2t_p$ linear clearance was also considered with a rectangular gusset plate.

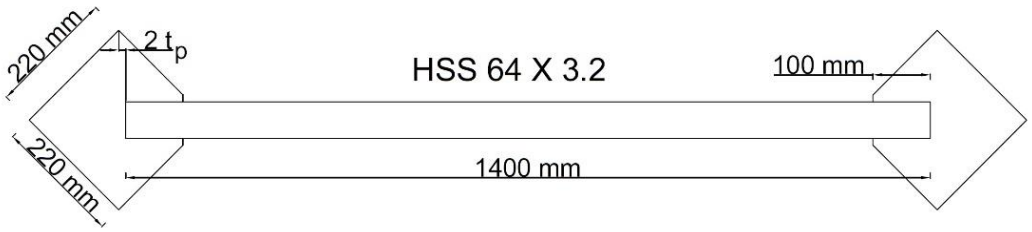

Figure 4.3: Steel tube brace with end gusset plates.

Finite element models were created for the numerical analysis using Abaqus. Shell elements with 5 integration points through the thickness were used to capture the stress-strain behavior in the elements. Smaller meshing was used in the middle length to capture local buckling and fracture (Figure 4.4). Fixed boundary conditions were imposed at the end of the gusset plates to resemble gusset-to-frame connection. To achieve numerical stability, initial imperfections were introduced in the form of a combination of the 1st and 2nd buckling modes with amplitudes of *B*/1000 and *B*/2000, respectively, where *B* is the brace length between the working points. The ductile fracture criterion was the same as used for the gusset plate study. The loading protocol from ATC24 [39] was used in the analysis.

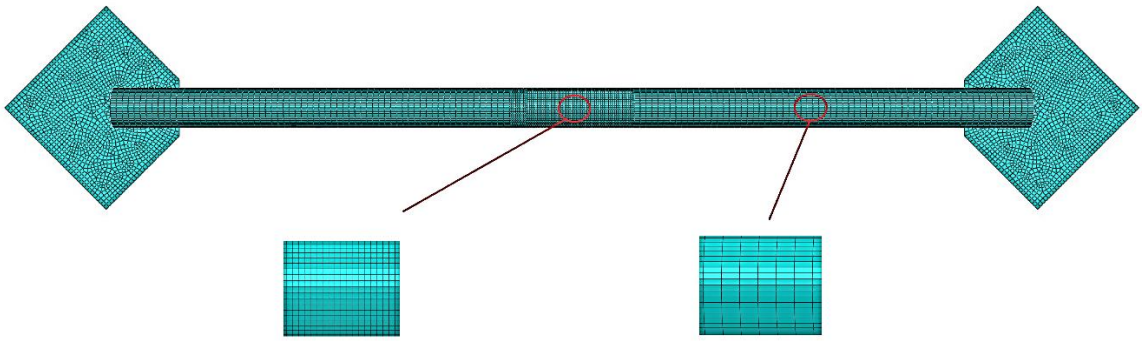

Figure 4.4: Finite element model of the specimen and the meshed regions.

4.3. Analysis Results

The axial force versus drift curves for all the specimens up to their maximum achieved drift ratios are presented in Figure 4.5. It should be noted that the maximum drift is defined as when the cracking initiates (the first element is deleted) in the models. The untreated specimen reached a maximum force of 250 kN, and cracking occurred at a story drift of 2.00%. The fully heat treated specimen reached a maximum force of 420 kN, almost 68% higher than the normal specimen. However, lower ductility of the heat treated steel resulted in a 37% reduction in maximum achieved drift. For Specimens R1 to R5, which were heat treated in ring shapes with different widths, the highest forces and the maximum achieved drift ratios varied depending on the length of the heat treated rings. For Specimen R1 with the widest rings, the maximum force was near 290 kN, and the maximum drift ratio was 1.25%. For Specimen R5, these amounts were 375 kN and 1.00%. This shows that while the wider rings resulted in relatively larger global ductility, it was still significantly less ductile than the untreated specimen. This is because the untreated specimen experienced global buckling, while the heat treated specimens of all ring widths experienced local

buckling instead (Figure 4.6). This is due to the tendency of the low-yield steel to experience nonlinear behavior and bulge while the heat treated steel ring is still in the linear phase [25]. Therefore, for Specimens R1 to R5, the deformation is concentrated in one of the rings, which leads to higher plastic deformation. As a result, the failure occurred earlier in the Specimens R1 to R5.

For the spiral-shape and cross-spiral heat treated braces, the maximum force remained similar to the untreated brace. However, the maximum drift ratios vary depending on the heat treatment design. Specimens S1 and S2 reached a drift ratio of 1.75%, which is 12.5% lower than the untreated specimen. For Specimen S3, the maximum drift ratio was 2.25%, which is slightly higher than the achieved drift of the untreated specimen. Specimen S4 reached a drift ratio of 1.25%, the lowest ductility among spiral-shape heat treated braces. Specimen CS1 reached a drift ratio of 2.00%, which is similar to the untreated specimen, and Specimen CS2 reached 1.75%, which is similar to Specimen S1 and S2. The results of spiral-shape and cross-spiral heat treated braces show that the spiral configuration plays a key role in determining the force-drift performance of the brace, and best performance is found with the smaller untreated width. Figure 4.6 shows that, unlike the ring-shape heat treated braces, the spiral-shape and cross-spiral heat treated braces experienced global buckling rather than local buckling, which leads to their comparatively better performance.

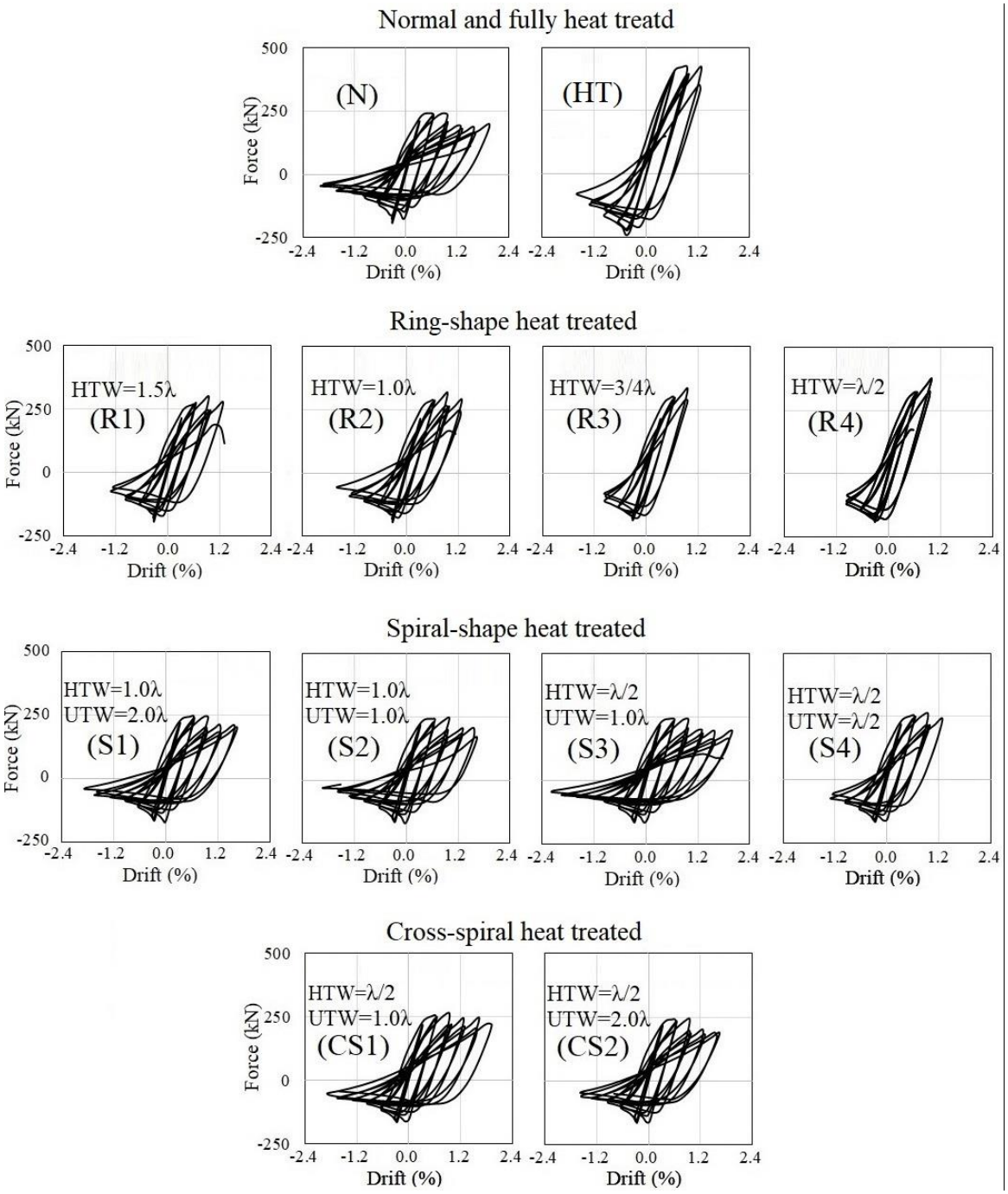

Figure 4.5: Force-drift curves of different cases (HTW and UTW stand for heat treated width and untreated width, respectively)

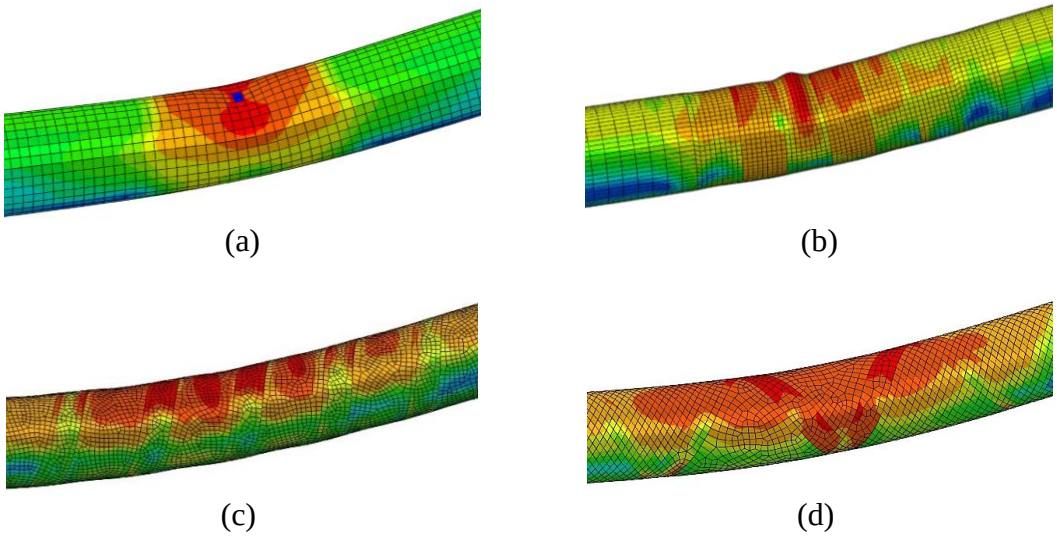

Figure 4.6: Buckling modes of Specimens: (a) Untreated and fully heat treated (b) Ring-shape heat treated (R2) (c) Spiral-shape heat treated (S3) (d) Cross-spiral heat treated (CS1)

The total hysteretic energy dissipated during the cyclic loading up to initiation of cracking is a good parameter to compare the performance of each specimen as large dissipated energy indicates ability to absorb earthquake energy to protect other structural and non-structural elements. This is related to the maximum forces in plastic deformation and drift ratios that each brace achieved, and is calculated from the area within the force-deformation hysteretic curve of the specimen. For each specimen, the dissipated energy is shown in Figure 4.7. It is seen that for fully heat treated specimen, HT, the dissipated energy was reduced by 24% compared to the untreated specimen, N. For the ring-shape heat treated specimens, R1 to R5, the energy dissipated before fracture is less than both the untreated and the fully heat treated specimens. This reduction in is most extreme for the specimens with a heat treated ring width lower than the local buckling wavelength, R3 to R5, almost

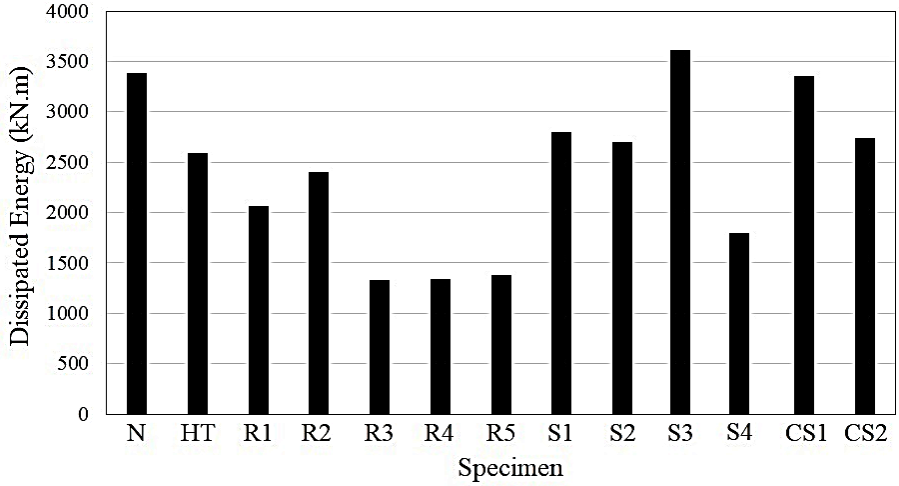

Figure 4.7: Dissipated hysteretic energy before initiation of cracking

59% lower than the normal specimen. For the spiral-shape and cross-spiral heat treated samples, S1 to CS2, the dissipated energy is highly dependent on the heat treated geometries. Specimen S3 showed the best performance with larger energy dissipated than the untreated specimen by 6%. For Specimen CS1, the dissipated energy was similar to the untreated specimen. Specimens S1, S2, and CS2 exhibited better energy dissipation capacity compared to the fully heat treated specimen, however, lower than the normal specimen by nearly 20%.

The results show that the performance of the braces is sensitive to the shape and arrangement of the heat treated paths. The ring-shape heat treated specimens all showed a reduction in final drift ratios and energy dissipation, which is a disadvantage. For the spiral-shape and cross-spiral heat treated specimens, the maximum force remained the same as the untreated brace for all heat treatment widths. However, the maximum drift ratios and energy dissipated before cracking was increased in Specimen S3, while it remained the same for Specimen CS1 and reduced for the other Specimens, S1, S2, S4 and CS2.

CHAPTER5: CONCLUSIONS AND RECOMMENDATIONS

In this thesis, heat treatment was proposed as a novel method to enhance the seismic behavior of CBFs. With heat treatment, the mechanical behavior of the steel element is changed locally with the aim of reducing damage in the brace-beam-column connection, achieving higher drift ratios, and increasing energy dissipation. To start, a series of material tests were conducted to study the effects of heat treatment protocols on samples of normal and high strength structural steels. The results of the microhardness and tensile tests showed that the tensile strength of the steel can be effectively reduced, by up to 50% for the high strength steel while ductility was increased by 98%. Larger strength reduction can be achieved through slower cooling rates and by starting with a higher strength steel rather than normal strength. The tensile strength of both the normal and high strength steel samples converged when the cooling rate was slower than 2 ºC/min.

A novel gusset plate design method using heat treated high strength steel was proposed to enhance the inelastic performance of gusset plate connections in CBFs under lateral loading. In this method, the failure mechanism is controlled and damage is substantially reduced compared with the conventional $2t_p$ fold line and $8t_p$ elliptical clearance design methods. A yield path was suggested by locally lowering the yield strength through heat treatment, shifting inelastic deformation away from the gusset-to-frame connection and concentrating it into the weakened region. High strength steel was used in the design to take advantage of the ability to significantly reduce its strength through controlled cooling.

After the material testing, various gusset plate connections were designed using normal steel, high strength steel, and heat treated high strength steel. The plates were modeled numerically to compare the behavior under cyclic loading. Using high strength steel led to 55% smaller gusset plate designs, with slightly larger sizes for the heat treated plates. While high strength steel gusset plates required the smallest dimensions, beneficial for construction, they did not perform as well as normal strength steel gusset plates due to local buckling from a combination of smaller cross-sectional stiffness and frame action. In the heat treated specimen, plastic deformation was successfully shifted away from the gusset-to-frame connection to the predetermined yield zone. This significantly delayed gusset plate and weld tearing near the beam and column connection zones compared to the normal strength gusset plates, which allowed the CBF with the heat treated plates to achieve higher drift ratios.

Heat treatment was then extended to steel tube braces, this time starting with normal steel and then the yield and ultimate strength was increased locally. Ring-shape, spiral-shape, and cross-spiral paths were suggested for the heat treated geometries with different heat treatment widths. Scaled braces with end gusset plate connections were designed and modeled numerically, and then subjected to cyclic loading. It was shown that the peak axial forces of the braces increased for the ring-shape heat treated specimens. However, the maximum achieved drift ratios and dissipated energy were reduced substantially due to concentration and localization of the plastic strain. For the spiral-shape and cross-spiral heat treated specimens, the maximum force did not change substantially, but the maximum achieved drift ratios and dissipated energy varied based on the width of heat treatment. The

maximum drift ratio and dissipated energy reduced for all specimens except the brace with spiral heat treatment with $\lambda/2$ width and untreated width of λ, which experienced a slight enhancement.

Altogether, for the ring-shape heat treated braces, the heat treatment failed to achieve higher drift ratio. For the spiral-shape and cross-spiral heat treated braces, heat treatment was slightly beneficial for one case, the brace with spiral heat treatment with $\lambda/2$ width. It can be inferred that, except the brace with spiral heat treatment with $\lambda/2$ width and untreated width of λ, for the other specimens as the untreated width gets smaller, the achieved drift ratio is reduced. With all this taken into account, for locally heat treated braces, the results highly depend on the heat treatment configuration.

5.1. Recommendations for Future Work

In gusset plate connections, using heat treatment resulted in an enhanced CBF connection performance while utilizing a smaller gusset plate; however, future studies on heat treatment geometry should be conducted to further improve performance to switch the failure mechanism to brace fracture in all cases. Various gusset plate dimensions and plate thicknesses as well as different cross-sections for the braces can be examined for this purpose. Experimental tests should also be done to further verify the numerical results and prove the practicality of performing heat treatment.

For the heat treated braces, the analysis results highly depend on the heat treatment configurations and widths. Further studies should concentrate on different material combinations such as starting with normal steel and using heat treatment with different

strengthening intensities, or starting with high strength steel sections and using heat treatment to reduce the strength locally with various strength reduction scenarios. This study only looked at circular tube sections; however, rectangular cross-sections are more frequently-used for braces. Thus, rectangular sections should be studied for similar heat-treated and untreated configurations. As rectangular section have problems with local buckling, localized heat treatment may be more beneficial for this application. Additionally, a range of tubular sections with different diameters and thicknesses should be studied, as the buckling behavior highly depends on the ratio of the diameter to thickness of the section.

REFERENCES

[1] C.W. Roeder, D.E. Lehman, K. Clark, J. Powell, J.H. Yoo, K.C. Tsai, C.H. Lin, and C.Y. Wei, Influence of gusset plate connections and braces on the seismic performance of X-braced frames. *Earthquake Engineering & Structural Dynamics*, 2011. **40**(4): p. 355-374.

[2] AISC, *Steel construction manual*. American Institute of Steel Construction. Chicago, 13th ed., 2005.

[3] CISC, *Handbook of steel construction*. Canadian Institute of Steel Construction. Toronto, 10th ed., 2011.

[4] F. Javidan, A. Heidarpour, X.-L. Zhao, and J. Minkkinen, Application of high strength and ultra-high strength steel tubes in long hybrid compressive members: Experimental and numerical investigation. *Thin-Walled Structures*, 2016. **102**: p. 273-285.

[5] G. Shi, K. Xu, H. Ban, and C. Lin, Local buckling behavior of welded stub columns with normal and high strength steels. *Journal of Constructional Steel Research*, 2016. **119**: p. 144-153.

[6] A. Ataei, M.A. Bradford, H.R. Valipour, and X. Liu, Experimental study of sustainable high strength steel flush end plate beam-to-column composite joints with deconstructable bolted shear connectors. *Engineering Structures*, 2016. **123**: p. 124-140.

[7] M. Morrison, D. Schweizer, and T. Hassan, An innovative seismic performance enhancement technique for steel building moment resisting connections. *Journal of Constructional Steel Research*, 2015. **109**: p. 34-46.

[8] Y. Yu, Z. Chen, and X. Wang, Investigation and evaluation of a novel technique on CFRT column connection. *Journal of Constructional Steel Research*, 2015. **113**: p. 195-208.

[9] M.L. Morrison, D.Q. Schweizer, and T. Hassan, Seismic enhancement of welded unreinforced flange-bolted web steel moment connections. *Journal of Structural Engineering*, 2016. **142**(11): p. 04016102.

[10] Y. Yu, Z. Chen, H. Liu, and X. Wang, Effects of strength-weakening oriented heat treatment on structural steel and its application on steel plate shear walls. *Construction Building Materials*, 2017. **151**: p. 827-839.

[11] MCASIS. McMaster University. 2018.

[12] A. Astaneh-Asl, Seismic behavior and design of gusset plates. Steel TIPS Report, 1998.

[13] A. Astaneh-Asl and S.C. Goel, Cyclic in-plane buckling of double angle bracing. *Journal of Structural Engineering*, 1984. **110**(9): p. 2036-2055.

[14] A. Astaneh-Asl, S.C. Goel, and R.D. Hanson, Cyclic out-of-plane buckling of double-angle bracing. *Journal of Structural Engineering*, 1985. **111**(5): p. 1135-1153.

[15] G. Martinez-Saucedo, J.A. Packer, and C. Christopoulos, Gusset plate connections to circular hollow section braces under inelastic cyclic loading. *Journal of Structural Engineering*, 2008. **134**(7): p. 1252-1258.
[16] D.E. Lehman, C.W. Roeder, D. Herman, S. Johnson, and B. Kotulka, Improved seismic performance of gusset plate connections. *Journal of Structural Engineering*, 2008. **134**(6): p. 890-901.
[17] J.H. Yoo, D.E. Lehman, and C.W. Roeder, Influence of connection design parameters on the seismic performance of braced frames. *Journal of Constructional Steel Research*, 2008. **64**(6): p. 607-623.
[18] J.H. Yoo, C.W. Roeder, and D.E. Lehman, Analytical performance simulation of special concentrically braced frames. *Journal of structural engineering*, 2008. **134**(6): p. 881-889.
[19] A. Watanabe, Y. Hitomi, E. Saeki, A. Wada, and M. Fujimoto. Properties of brace encased in buckling-restraining concrete and steel tube. in *Proceedings of ninth world conference on earthquake engineering*. 1988.
[20] H. Mohammadi, V. Toufigh, A.A. Golafshani, and A. Arzeytoon, Experimental evaluation of pinned frame equipped with ribbed bracing system. *Journal of Earthquake Engineering*, 2017: p. 1-21.
[21] R. Tremblay and A. Filiatrault, Seismic impact loading in inelastic tension-only concentrically braced steel frames: myth or reality? *Earthquake engineering and structural dynamics*, 1996. **25**(12): p. 1373-1389.
[22] R. Shepherd, Multiphase cross bracing in earthquake resistant structures. *Earthquake Engineering and Structural Dynamics*, 1972. **4**: p. 311-324.
[23] P. C. Hsiao, K. Hayashi, H. Inamasu, Y.-B. Luo, and M. Nakashima, Development and testing of naturally buckling steel braces. *Journal of Structural Engineering*-Asce, 2015. **142**(1): p. 04015077.
[24] K.A. Skalomenos, M. Kurata, H. Shimada, and M. Nishiyama, Use of induction-heating in steel structures: Material properties and novel brace design. *Journal of Constructional Steel Research*, 2018. **148**: p. 112-123.
[25] F. Siska, M. Ramajayam, D. Fabijanic, and M.J.A.M. Barnett, Internal material "architecture" for a kink-resistant metal tube. *Acta Materialia*, 2013. **61**(1): p. 331-340.
[26] K. Andrews, Empirical formulae for the calculation of some transformation temperatures. *Journal of the Iron and Steel Institute*, 1965: p. 721-727.
[27] J. Barralis and G. Maeder, Métallurgie Tome I: Métallurgie Physique. *Collection Scientifique ENSAM*, 1982: p. 270.
[28] R. Grange, Estimating critical ranges in heat treatment of steels, in *Metal Progress*. 1961. p. 73-75.
[29] C.W. Roeder, E.J. Lumpkin, and D.E. Lehman, A balanced design procedure for special concentrically braced frame connections. *Journal of Constructional Steel Research*, 2011. **67**(11): p. 1760-1772.
[30] J.A. Powell, Evaluation of special concentrically braced frames for improved seismic performance and constructability. M.Sc. thesis, 2010, University of Washington.

[31] K. Khandelwal, S. El-Tawil, and F. Sadek, Progressive collapse analysis of seismically designed steel braced frames. *Journal of Constructional Steel Research*, 2009. **65**(3): p. 699-708.
[32] NIST. (2010), Evaluation of the FEMA P695 methodology for quantification of building seismic performance factors. NEHRP Consultants Joint Venture, Gaithersburg, MD. 2010.
[33] ABAQUS Analysis User's Manual. Dassault Systemes Simulia Corp. Simulia DCS, Providence, RI, US. 2014.
[34] A. Prantl, J. Ruzicka, M. Spaniel, M. Moravec, J. Dzugan, and P. Konopík. Identification of ductile damage parameters. in *SIMULIA Community Conference*. 2013. Vienna, Austria.
[35] Y. Bai and T. Wierzbicki, A comparative study of three groups of ductile fracture loci in the 3D space. *Engineering Fracture Mechanics*, 2015. **135**: p. 147-167.
[36] J.R. Rice and D.M. Tracey, On the ductile enlargement of voids in triaxial stress fields∗. *Journal of the Mechanics Physics of Solids*, 1969. **17**(3): p. 201-217.
[37] V.V. Saykin, J. Song, and J. Hajjar, A validated approach for modeling collapse of steel structures, Department of Civil and Environmental Engineering Reports. 2014, Citeseer, Northeastern University, Boston, Massachusetts.
[38] B.V. Fell, Large-scale testing and simulation of earthquake-induced ultra low cycle fatigue in bracing members subjected to cyclic inelastic buckling. PhD dissertation, 2008, University of California, Davis.
[39] H. Krawinkler, Guidelines for cyclic seismic testing of components of steel structures for buildings, ATC-24. 1992: Redwood City, California.
[40] C. DesForges, Laser heat treatment. *TRIBOLOGY international*, 1978. **11**(2): p. 139-143.

APPENDIX A: GUSSET PLATE DESIGN EXAMPLE

This appendix provides a design example to show the procedure used to design gusset plates made of normal steel, high strength steel, and heat treated high strength steel. These examples generally follow Balanced Designed Procedure introduced earlier in the text, and the Canadian steel design code (S16-14) is used to check and control additional design details. The calculations presented here are for designing Case 3 (from Table 3.1 in the text) with the member sections shown in Figure A.1.

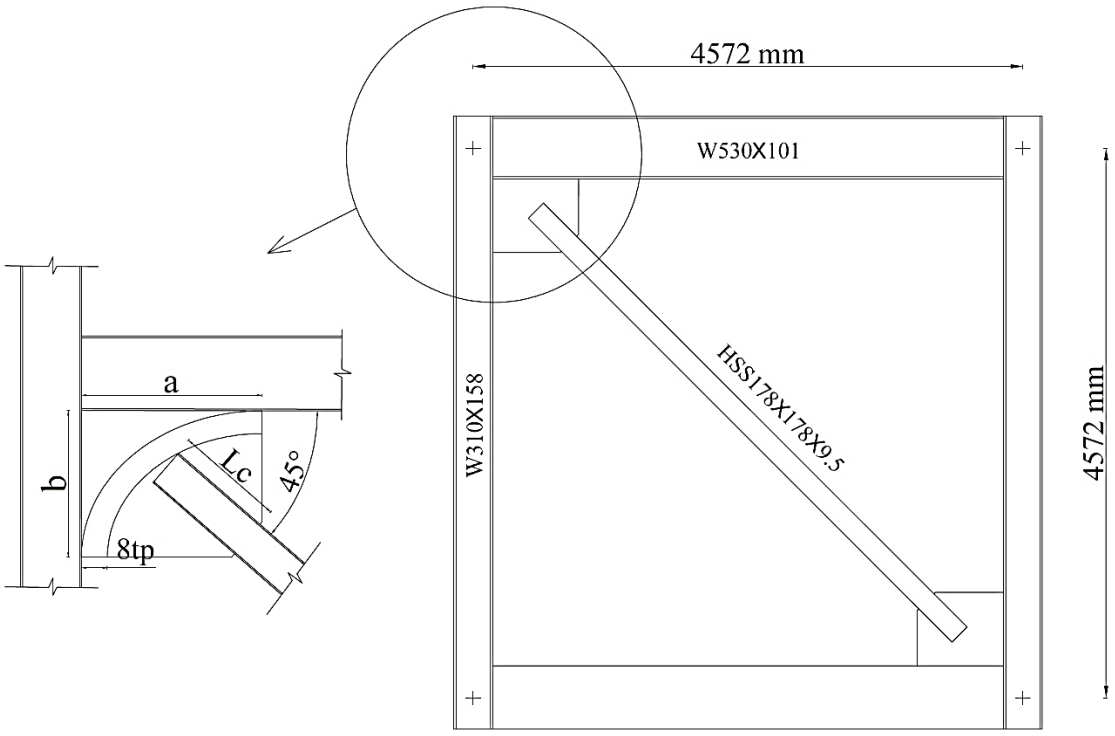

Figure A.1: Section profiles of Case 3 frame.

Symbol Definitions

A_g	Gross cross-sectional area of the brace
A_{nb}	Net area of the brace
B	Brace width
B_W	Whitmore width
E	Modulus of elasticity
F_{cr}	Critical buckling stress
F_e	Euler buckling stress
F_{EXX}	Electrode strength
F_y	Yield strength of steel
Fu	Ultimate strength of steel
Hb	Horizontal force of gusset plate to beam
Hc	Horizontal force of gusset plate to column
K	Effective length coefficient
L	Brace length
Lc	Brace-to-gusset connection length
L_{avg}	Average buckling length in gusset plate
L_{nv}	Length of gross area of brace in shear
Ns	Number of shear planes
N_w	Number of weld lines
P_{uc}	Maximum expected compressive capacity of brace
P_{ut}	Maximum expected tensile capacity of brace
R_y	Ratio of the expected to the specified yield stress of steel
U_{bs}	AISC shear lag factor
Vb	Vertical force of gusset plate to beam
Vc	Vertical force of gusset plate to column
a	Length of gusset plate
b	Height of gusset plate
r	Radius of gyration
e_b	Half of the beam height
e_c	Half of the column height
t_p	Gusset plate thickness
w_1	Interface weld size
w_2	Brace-to-gusset weld leg size
$\bar{x}$	Connection eccentricity
θ	The angle between the brace and the beam
φ	Resistance factor
β	Balance factor

A.1. Design of Normal Steel Gusset Plate

Here, the balanced design procedure for designing the gusset plate is followed. The material properties are

$$F_y = 350\ MPa, Fu = 450\ MPa$$

1. The expected tensile capacity of the brace is

$$A_g = 6180\ mm^2, r = 68\ mm$$

$$P_{ut} = R_y F_y A_g = (1.4)(350)(6180) = 3028\ kN$$

2. The length of brace-to-gusset plate weld is found by checking the weld strength

$$L_c = \frac{P_{ut}}{\beta(0.6)F_{EXX}N_W(0.707)w_2} = \frac{3028000}{0.75(0.6)490(4)0.707(10)} = 388\ mm$$

3. The weld length must be double checked for the brace base material strength

$$0.75(0.6)F_u N_c L_c t_f = 0.75(0.6)450(4)388(9.5) = 3091 > P_{ut}$$

4. The Whitmore width of the plate is

$$B_W = 178 + 2(388)\tan(30) = 626$$

And the gusset plate thickness, t_p, is found by checking three criteria

Yielding capacity:

$$t_p \geq \frac{P_{ut}}{\beta R_y F_y B_W} = \frac{3028000}{0.75(1.1)350(626)} = 16.75\ mm$$

Tensile capacity:

$$t_p \geq \frac{P_{ut}}{\beta F_u B_W} = \frac{3028000}{0.85(450)626} = 12.65\ mm$$

Block shear capacity:

$$t_p \geq \frac{P_{ut}}{\beta F_u (0.6L_{nv} + U_{bs}B)} = \frac{3028000}{0.85(450)(0.6(2)388 + 1(178))} = 12.3\ mm$$

Choose $t_p = 17\ mm$

5. The dimensions of the gusset plate are derived graphically by considering the $8t_p$ (136 mm) elliptical clearance and the connection length, L_c

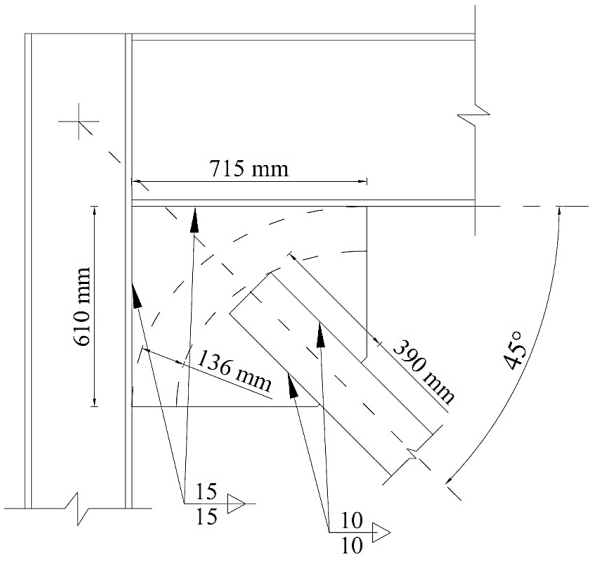

The Generalized Uniform Force Method is used to size the gusset plate. Based on this method, there is no constraint formula to size the gusset plate. Instead, the gusset plate dimensions are specified first, and the forces on the adjacent beam and column imposed from the gusset plate are calculated using these formulas

$$H_c = \frac{e_c Cos\theta}{e_b + \frac{b}{2}} P_{ut} = \frac{\frac{327}{2} Cos45}{\frac{537}{2} + \frac{610}{2}} (3028000) = 610kN$$

$$V_b = \frac{e_b (Sin\theta \left(e_b + \frac{b}{2}\right) - e_c Cos\theta)}{\frac{a}{2}(e_b + \frac{b}{2})} P_{ut} = \frac{\frac{537}{2}(Sin45\left(\frac{537}{2} + \frac{610}{2}\right) - \frac{327}{2} Cos45)}{\frac{715}{2}\left(\frac{537}{2} + \frac{610}{2}\right)} (3028000) = 1150\ kN$$

$$H_b = P_{ut} Sin\theta - H_c = 1531\ kN$$

$$V_c = P_{ut} Cos\theta - V_b = 991\ kN$$

These forces can be used for the design of the welds.

6. The buckling capacity of the brace is

$$F_e = \frac{\pi^2 E}{\left(\frac{KL}{r}\right)^2} = \frac{\pi^2 (200000)}{\left(\frac{4990}{68}\right)^2} = 367\ MPa$$

$$F_{cr} = \left(0.658^{\frac{R_y F_y}{F_e}}\right) F_y = \left(0.658^{\frac{1.4(350)}{367}}\right) 350 = 200\ MPa$$

$$P_{uc} = 1.1 R_y F_{cr} A_g = 1.1(1.4)200(6180) = 1903\ kN$$

7. The gusset plate buckling capacity is then checked

$$L_{avg} = \frac{L_1 + L_2 + L_3}{3} = \frac{371 + 57 + 198}{3} = 209\ mm$$

$$\frac{KL_{avg}}{r} = \frac{0.65(209)}{\frac{17}{\sqrt{12}}} = 27.7$$

$$F_e = \frac{\pi^2 E}{\left(\frac{KL_{avg}}{r}\right)^2} = \frac{\pi^2 (200000)}{(27.7)^2} = 2573\ MPa$$

The buckling capacity of the gusset plate should be higher than the brace

$$\beta B_W t_p F_{cr} = 0.9(626)17\left(0.658^{\frac{1.4(350)}{2573}}\right)350 = 3095\ kN > P_{uc} = 1903\ kN$$

8. The interface welds between the gusset plate and the adjacent beam and columns is designed by

$$w_1 > \frac{R_y F_y t_p}{2(1.2)\beta(0.6)F_{EXX}(0.707)} = \frac{1.1(350)17}{2(1.2)0.75(0.6)490(0.707)} = 17\ mm$$

A 17-mm fillet weld on each side should be used over the full length of the interface.

9. Net section reinforcement is designed by a 100-mm wide plate with a length of 300 mm and a thickness of 10 mm is used as the net section reinforcement. The slot in the brace is cut 5 mm thicker for a better erection practicality.

$$\bar{x} = \frac{184(9.5)96.75 + 2(93)9.5(55)}{184(9.5) + 2(93)9.5} = 75.76$$

$$A_{nb} = 6180 - 2(17 + 5)(9.5) = 5762$$

$$A_{gv} = 100(10)2 = 2000\ mm^2$$

$$U = 1 - \frac{\bar{x}}{L} = 1 - \frac{75.76}{300} = 0.75$$

$$\beta U\left(R_{tb}F_{ub}A_{nb} + F_{up}A_{gv}\right) = 0.95(0.75)\left(1.3(450)5762 + 450(2000)\right) = 3043kN$$

$$> P_{ut} = 3028\ kN \qquad \text{The condition is met.}$$

A.2. Design of High Strength Steel Gusset Plate

This gusset plate has A514 steel, the material properties of which are

$$F_y = 690\ MPa, Fu = 760\ MPa$$

1. The expected tensile capacity of the brace is

$$P_{ut} = 3028\ kN$$

2. The length of brace-to-gusset plate weld is found by checking the weld strength

$$L_c = \frac{P_{ut}}{\beta(0.6)F_{EXX}N_W(0.707)w_2} = \frac{3028000}{0.75(0.6)820(4)0.707(10)} = 232\ mm$$

3. The weld length must be double checked for the brace base material strength

$$0.75(0.6)F_uN_sL_st_f = 0.75(0.6)450(4)232(9.5) = 1848 < P_{ut}$$

The condition is not met. Therefore, the same L_c which was used for the normal steel is used for high strength steel:

$$L_c = 388\ mm$$

4. The Whitmore width of the plate is

$$B_W = 178 + 2(388)\tan(30) = 626$$

And the gusset plate thickness, t_p, is found by checking three criteria

Yielding capacity:

$$t_p \geq \frac{P_{ut}}{\beta R_y F_y B_W} = \frac{3028000}{0.75(1.1)690(626)} = 8.50\ mm$$

Tensile capacity:

$$t_p \geq \frac{P_{ut}}{\beta F_u B_W} = \frac{3028000}{0.85(760)626} = 7.49\ mm$$

Block shear capacity:

$$t_p \geq \frac{P_{ut}}{\beta F_u (0.6L_{nv} + U_{bs}B)} = \frac{3028000}{0.85(760)\big(0.6(2)388 + 1(178)\big)} = 7.28\ mm$$

Choose $t_p = 10\ mm$

It should be noted that the first choice for t_p was 9 mm. Then, buckling was observed in Abaqus models, although the calculations for the compressive strength had shown that the buckling capacity of the gusset plate was sufficient. As a result, the thickness was increased to 10 mm to prevent buckling in the gusset plates.

5. The dimensions of the gusset plate is found by

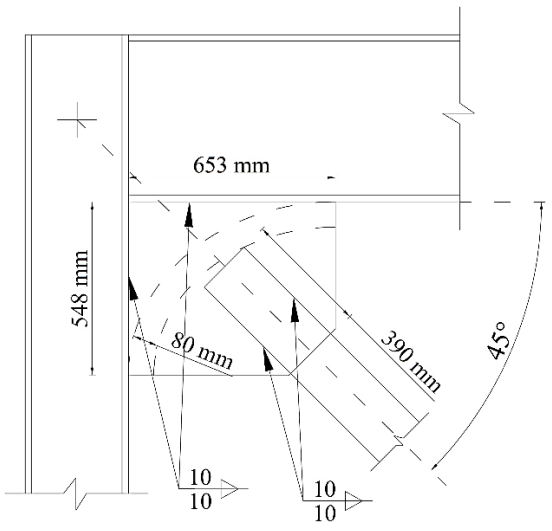

6. The buckling capacity of the brace is found by

$$F_e = \frac{\pi^2 E}{\left(\frac{KL}{r}\right)^2} = \frac{\pi^2(200000)}{\left(\frac{5152}{68}\right)^2} = 344\ MPa$$

$$F_{cr} = \left(0.658^{\frac{R_y F_y}{F_e}}\right) F_y = \left(0.658^{\frac{1.4(350)}{344}}\right) 350 = 193\ MPa$$

$$P_{uc} = 1.1 R_y F_{cr} A_g = 1.1(1.4)193(6180) = 1837\ kN$$

7. The gusset plate buckling capacity is then checked

$$L_{avg} = \frac{L_1 + L_2 + L_3}{3} = \frac{290 + 111 + 0}{3} = 134\ mm$$

$$\frac{KL_{avg}}{r} = \frac{0.65(134)}{\frac{10}{\sqrt{12}}} = 30.17$$

$$F_e = \frac{\pi^2 E}{\left(\frac{KL_{avg}}{r}\right)^2} = \frac{\pi^2 (200000)}{(30.17)^2} = 2169\ MPa$$

The buckling capacity of the gusset plate should be higher than the brace

$$\beta B_W t_p F_{cr} = 0.9(626)10\left(0.658^{\frac{1.4(690)}{2169}}\right)690 = 3226\ kN > P_{uc} = 1837\ kN$$

8. The interface welds between the gusset plate and the adjacent beam and columns is designed

$$w_1 > \frac{R_y F_y t_p}{2(1.2)\beta(0.6)F_{EXX}(0.707)} = \frac{1.1(690)10}{2(1.2)0.75(0.6)820(0.707)} = 10\ mm$$

A 10-mm fillet weld on each side should be used over the full length of the interface.

9. Net section reinforcement is designed by

A 100-mm wide plate with a length of 300 mm and a thickness of 10 mm is used as the net section reinforcement.

A.3. Design of Heat Treated High Strength Steel Gusset Plate

The material property of A514 after heat treatment

$$F_{yH} = 380\ MPa, Fu = 510\ MPa$$

1. The expected tensile capacity of the brace is

$$P_{ut} = 3028\ kN$$

2. The length of brace-to-gusset plate weld is found by checking the weld strength

$$L_c = \frac{P_{ut}}{\beta(0.6)F_{EXX}N_W(0.707)w_2} = 232\ mm$$

3. The weld length must be double checked for the brace base material strength

$$0.75(0.6)F_u N_c L_s t_f = 0.75(0.6)450(4)232(9.5) = 1848 < P_{ut}$$

   The condition is not met. Therefore, the same L_c which was used for the normal steel is used for heat treated high strength steel

$$L_c = 388\ mm$$

4. In this stage, we need to know the length of critical tensile yielding area of the HTZ, L_H. However, this parameter is extracted graphically from the gusset plate drawing, which is unknown in this stage. Hence, as a trial and error method, first we suppose that

$$L_H = B_W = 178 + 2(388)\tan(30) = 626\ mm$$

   And the gusset plate thickness, t_p, is found by checking three criteria

   Yielding capacity:

$$t_p \geq \frac{P_{ut}}{\beta R_y F_y B_W} = \frac{3028000}{0.75(1.1)380(626)} = 14.0\ mm$$

Tensile capacity:

$$t_p \geq \frac{P_{ut}}{\beta F_u B_W} = \frac{3028000}{0.85(760)626} = 11.16\ mm$$

Block shear capacity is controlled through

$$t_p \geq \frac{P_{ut}}{\beta F_u (0.6L_{nv} + U_{bs}B)} = \frac{3028000}{0.85(760)\big(0.6(2)388 + 1(178)\big)} = 7.28\ mm$$

Choose $t_p = 14\ mm$

5. The dimensions of the gusset plate is found by

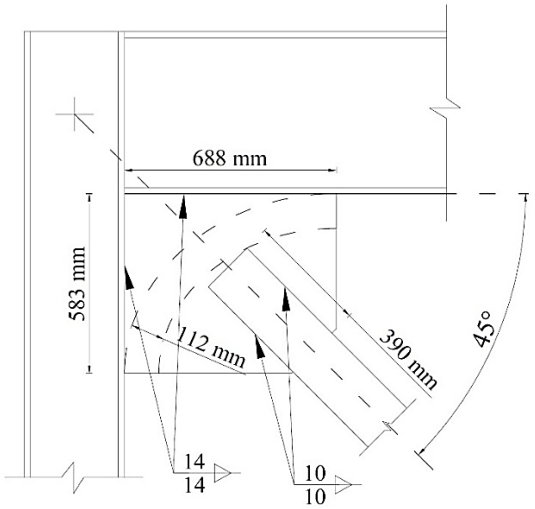

Now L_H can be measured graphically from the drawing, which is: $L_H = 628\ mm$

Since it is very close to the assumption, 626 mm, the condition is met and the plate thickness is sufficient.

6. The buckling capacity of the brace is found by

$$F_e = \frac{\pi^2 E}{\left(\frac{KL}{r}\right)^2} = \frac{\pi^2(200000)}{\left(\frac{5152}{68}\right)^2} = 344\ MPa$$

$$F_{cr} = \left(0.658^{\frac{R_y F_y}{F_e}}\right) F_y = \left(0.658^{\frac{1.4(350)}{344}}\right) 350 = 193\ MPa$$

$$P_{uc} = 1.1 R_y F_{cr} A_g = 1.1(1.4)193(6180) = 1837\ kN$$

7. The gusset plate buckling capacity is then checked

$$L_{avg} = \frac{L_1 + L_2 + L_3}{3} = \frac{290 + 111 + 0}{3} = 134\ mm$$

$$F_e = \frac{\pi^2 E}{\left(\frac{KL_{avg}}{r}\right)^2} = \frac{\pi^2(200000)}{\left(\frac{0.65(134)}{\frac{10}{\sqrt{12}}}\right)^2} = 2169\ MPa$$

The buckling capacity of the gusset plate should be higher than the brace

$$\beta B_W t_p F_{cr} = 0.9(626)10\left(0.658^{\frac{1.4(690)}{2169}}\right)690 = 3226\ kN > P_{uc} = 1837\ kN$$

8. The interface welds between the gusset plate and the adjacent beam and columns is designed by

$$w_1 > \frac{R_y F_y t_p}{2(1.2)\beta(0.6)F_{EXX}(0.707)} = \frac{1.1(690)10}{2(1.2)0.75(0.6)820(0.707)} = 10\ mm$$

A 10-mm fillet weld on each side should be used over the full length of the interface.

9. A 100-mm wide plate with a length of 300 mm and a thickness of 10 mm is used as the net section reinforcement.